Materials Today Sustainability 35 (2026) 101430

Contents lists available at ScienceDirect

Materials Today Sustainability

journal homepage: www.journals.elsevier.com/materials-today-sustainability

Ionic thermoelectric geopolymers: Mechanisms, materials design, and device integration

Zhiyang Pei [a,1], Hanyun Hu [a,1], Jiaming Gu [b], Jingming Cai [a,c,*], Y.X. Zhang [c,**]

[a] School of Civil Engineering, Southeast University, Nanjing, 210000, China
[b] Department of Civil and Environmental Engineering, Faculty of Science and Technology, University of Macau, Macao Special Administrative Region of China
[c] School of Electrical, Mechanical and Biomedical Engineering, Faculty of Engineering and Information Technology, University of Technology Sydney, 81 Broadway, Ultimo, NSW, 2007, Australia

ARTICLE INFO

Keywords:
Geopolymer
Ionic thermoelectrics
Low-carbon binders
Low-grade heat harvesting
Self-powered sensing
Sustainable infrastructure

ABSTRACT

The global transition toward low-carbon urban infrastructure has positioned geopolymers as promising alternative binders for the built environment. Their three-dimensional aluminosilicate framework and tunable pore-solution environment offer opportunities for structure-integrated thermoelectric functions. This review synthesizes geopolymer-based thermoelectric materials by integrating transport mechanisms, materials design strategies, and device integration into a unified framework. The review examines how pore-solution ion transport, binder microstructure, composite pathways, and electrode-related interfacial processes collectively shape the apparent thermoelectric response. Strategies for modulating the apparent Seebeck coefficient, effective electrical conductivity, and thermal conductivity, from ionic regulation to microstructural and composite engineering, are critically evaluated in light of intrinsic trade-offs. Device-level demonstrations and integration requirements are further examined, including electrode-binder interfaces, moisture-regulated packaging, construction compatibility, and application-oriented evaluation for low-power functions. Sustainability considerations are discussed in relation to module-level carbon- and energy-burden screening, industrial by-product precursors, and reduced reliance on critical or supply-constrained thermoelectric elements. Finally, future directions are outlined to shift from material-centric optimization toward stable, low-power thermoelectric components designed for infrastructure-integrated sensing and localized energy harvesting.

1. Introduction

Climate change mitigation has intensified interest in low-carbon energy strategies within the built environment [1]. At the same time, global energy-related carbon emissions remain at historically high levels, reaching 37.8 Gt in 2024 according to the International Energy Agency [2]. In urban areas, large amounts of low-grade thermal energy are continuously generated and stored in buildings, pavements, and transport infrastructure due to solar radiation and anthropogenic heat. This phenomenon is further amplified by the urban heat island effect, which typically results in urban air temperatures being several degrees higher than those in surrounding rural areas [3–6]. The large thermal mass of urban infrastructure allows cities to accumulate and release considerable amounts of low-grade heat. The challenge is therefore not the availability of thermal energy, but how such dispersed heat can be effectively recovered within infrastructure systems. Various renewable technologies have been deployed in the built environment, including wind power, photovoltaic systems, and ground-source heat pumps [7]. However, these systems often face practical constraints when integrated into large-scale infrastructure. Their performance is strongly dependent on environmental conditions, and many systems involve mechanical components that require periodic maintenance during long-term operation [8,9]. Such limitations are particularly relevant for infrastructure applications, where long-term reliability, durability, and minimal operational intervention are essential.

Thermoelectric (TE) technology offers a solid-state approach for converting temperature gradients directly into electrical energy. Because thermoelectric systems operate without moving parts, they

* Corresponding author.
** Corresponding author.
E-mail addresses: jingmingcai@seu.edu.cn (J. Cai), Sarah.Zhang@uts.edu.au (Y.X. Zhang).
[1] These authors contributed equally to this work.

https://doi.org/10.1016/j.mtsust.2026.101430
Received 19 May 2026; Received in revised form 21 July 2026; Accepted 5 August 2026
Available online 5 August 2026
2589-2347/© 2026 The Authors. Published by Elsevier Ltd. This is an open access article under the CC BY-NC license (http://creativecommons.org/licenses/by-nc/4.0/).

enable silent operation, low mechanical wear, and potentially favorable long-term reliability [10,11]. These characteristics make thermoelectric technology attractive for the built environment, where small but persistent temperature differences can arise across building envelopes, pavements, and subsurface structures. Recent studies have explored thermoelectric generators for localized power supply and energy harvesting in infrastructure systems, including applications in self-powered sensing and thermal monitoring networks [12,13].

Despite this potential, large-scale deployment of thermoelectric technology in infrastructure remains limited by material constraints [14]. Conventional thermoelectric materials such as bismuth telluride (Bi_2Te_3) are costly, rely on relatively scarce elements, and exhibit poor compatibility with structural materials [15,16]. In addition, the overall cost associated with module fabrication, encapsulation, and long-term stability requirements remains prohibitive for large-area infrastructure applications [17–19]. These limitations have motivated increasing interest in developing low-cost thermoelectric materials compatible with construction systems.

Since the 1980s, cementitious materials have been explored as potential thermoelectric matrices, typically through the incorporation of conductive fillers or semiconducting phases [20]. However, two persistent challenges remain. First, cement-based thermoelectric materials are intrinsically heterogeneous, consisting of crystalline hydration products, amorphous gels, pore solution, and dispersed fillers, making their thermoelectric response difficult to interpret using conventional transport frameworks. As noted by Liu et al., performance improvements in such systems have largely relied on empirical optimization rather than binder-level mechanistic understanding [21]. Second, the thermoelectric response of ordinary cement-based matrices in early studies remained relatively limited, with reported apparent Seebeck coefficients often at the level of only a few microvolts per kelvin [22,23]. A notable shift emerged around 2020, when Cai et al. reported that geopolymers and alkali-activated binders could exhibit substantially enhanced thermoelectric responses compared with conventional cementitious materials [24]. This behavior is associated with the distinct structural characteristics of geopolymers. Unlike cement hydrates, geopolymers form amorphous aluminosilicate networks composed of interconnected $[SiO_4]$ and $[AlO_4]$ tetrahedra, creating polymerized frameworks that contain ion-transport pathways [25,26]. Their composition and internal structure can also be systematically tailored through precursor selection, mix design, and activation conditions [27]. As a result, geopolymer-based systems have been reported to exhibit apparent Seebeck coefficients one to two orders of magnitude higher than those typically observed in conventional cement-based materials [28,29]. These findings suggest that geopolymers may serve not only as structural binders but also as functional materials capable of measurable thermoelectric response, opening opportunities for low-cost thermoelectric materials compatible with construction applications.

Although several recent reviews have discussed thermoelectric cementitious composites and functional geopolymer materials [21,30], a focused synthesis of geopolymer-based ionic thermoelectric systems from the perspective of binder chemistry, ion-mediated transport, device integration, and sustainability remains limited. Existing discussions have largely situated geopolymer thermoelectrics within broader cementitious composite systems [20,31], while the reported thermoelectric response of geopolymer binders is closely related to their pore-solution chemistry, charged aluminosilicate frameworks, moisture-dependent ion transport, and electrode boundary conditions. Accordingly, this review focuses on geopolymer binders and examines how binder-level mechanisms influence performance interpretation, materials design, device evaluation, and sustainability considerations for infrastructure deployment.

Building on this scope, the review summarizes material systems, transport mechanisms, reported performance, and enhancement strategies in geopolymers and related alkali-activated binders, before discussing device-level concepts and practical constraints for low-carbon built environments. These interrelated dimensions are summarized in the conceptual framework shown in Fig. 1. The aim is to clarify the scientific basis and future development pathways of geopolymer-based thermoelectric materials as low-carbon functional binders.

2. Current research landscape of thermoelectric geopolymers

Geopolymers were originally developed as alternative inorganic binders for construction applications, with the concept first proposed by Davidovits in the late 1970s [32]. They have since been widely investigated as low-carbon binders because of their potential for reduced embodied carbon, high early strength, chemical resistance, and durability in aggressive environments [33]. Unlike ordinary Portland cement, geopolymer binders are synthesized through alkali activation rather than high-temperature clinker production, which can reduce CO_2 emissions associated with binder manufacture, depending on precursor source, activator production, and curing route [34]. From a materials perspective, geopolymers differ from Portland cement-based binders in both chemistry and structure. Whereas cement hydration products are mainly composed of calcium-rich hydrate assemblages, geopolymers form polymerized aluminosilicate networks through the polycondensation of reactive precursors [35]. These structural characteristics have traditionally been exploited for structural and durability applications and have more recently attracted attention for functional properties [36], including thermoelectric behavior. Consequently, geopolymer thermoelectrics have emerged at the intersection of alkali-activated materials, functional construction materials, and low-grade heat utilization.

2.1. Material systems of geopolymer thermoelectrics

Geopolymers are generally defined as inorganic aluminosilicate binders formed through the alkali activation of precursor materials such as metakaolin, fly ash, slag, and other industrial by-products [32,37]. Their formation typically involves dissolution of reactive aluminosilicate species, reorientation of dissolved units, and subsequent solidification into a polymerized geopolymer framework, as schematically illustrated in Fig. 2a [38]. At the atomic scale, the resulting structure consists of interconnected $[SiO_4]$ and $[AlO_4]$ tetrahedra forming three-dimensional networks that are charge-balanced by alkali cations [41,42]. Depending on precursor composition, these binders may exhibit different local structural environments and non-bridging oxygen configurations, particularly between low-calcium and high-calcium systems (Fig. 2b). Compared with Portland cement hydrates dominated by calcium silicate hydrate phases, many geopolymer binders therefore present a more continuous aluminosilicate framework with distinct structural organization [43]. After hardening, the geopolymer matrix comprises an aluminosilicate gel network together with ion-containing pore solution (Fig. 2c), which is closely related to subsequent charge transport behavior.

The precise definition of geopolymers remains subject to discussion. While some researchers restrict the term to metakaolin-based aluminosilicate systems, others extend it to include a broader class of alkali-activated materials derived from fly ash, slag, red mud, and other aluminosilicate-rich precursors [44,45]. In this review, geopolymer-based systems refer to aluminosilicate-rich alkali-activated binders and their composites when the hardened matrix is mainly governed by geopolymeric or alkali-activated aluminosilicate networks, ion-containing pore solution, and binder-level charge transport. This scope does not extend to ordinary Portland cement-dominated thermoelectric composites.

2.2. Processing routes and compositional design

In thermoelectric studies, geopolymer binders are typically synthesized through alkali activation using sodium- or potassium-based alkali

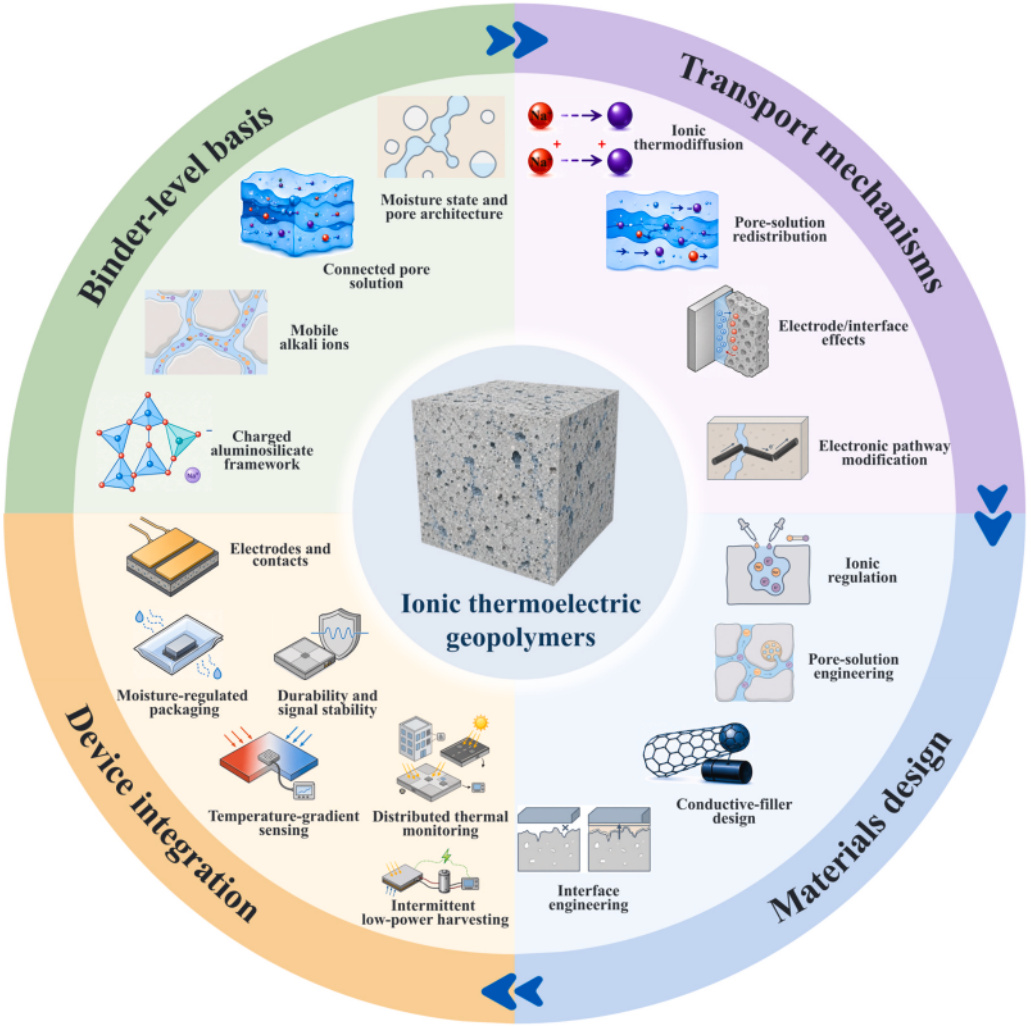


Fig. 1. Conceptual framework of ionic thermoelectric geopolymers, linking the binder-level basis and transport mechanisms with materials design, device integration, and low-power functions.

activators, including hydroxides and alkali silicates [46]. The activator composition, concentration, and silicate modulus influence precursor dissolution, gel formation, pore-solution chemistry, and the resulting network structure [47,48]. Fabrication generally follows conventional geopolymer processing routes, including precursor preparation, alkali activation, mixing, casting, and curing [49]. The resulting binder structure is governed by precursor reactivity, activator chemistry, water content, and curing conditions.

Compared with traditional cementitious systems, geopolymer processing provides considerable compositional and structural tunability. Precursor selection, alkali species, curing conditions, and mix design can be adjusted to modify the ionic environment, pore structure, and microstructure within the binder matrix [50]. This flexibility has long been exploited for tailoring mechanical performance and durability, and more recently has provided opportunities to regulate transport properties relevant to thermoelectric behavior. However, differences in activator chemistry, curing history, water content, and post-curing moisture state also contribute to substantial variability in reported thermoelectric performance. These processing-related factors should therefore be considered when comparing data across different studies.

2.3. Thermoelectric characterization methods

The characterization of thermoelectric properties in geopolymer systems differs from that used for conventional dense thermoelectric materials. For classical thermoelectric compounds such as intermetallic alloys and chalcogenides, standardized measurement systems are widely available [51]. In contrast, thermoelectric testing of geopolymer binders generally relies on customized experimental setups adapted from cementitious or electrochemical testing methods. The reported Seebeck coefficient, denoted here as the apparent Seebeck coefficient (S), is typically determined from the relationship between thermovoltage and the applied temperature difference across a specimen using customized heating-cooling setups [52,53]. In ion-conducting geopolymer systems, this value represents an apparent thermoelectric response because it may include contributions from ionic thermodiffusion, pore-solution redistribution, electrode boundary effects, and interfacial polarization. Effective electrical conductivity (σ) is commonly measured using two-probe or four-probe direct-current methods, as well as impedance-based methods, providing an effective conductivity that may include both ionic and electronic contributions [54,55]. Thermal conductivity (κ) measurements are less frequently reported and are often conducted using non-standard setups adapted from cementitious testing. Fig. 2d–f summarizes these measurement schemes.

As a result, complete datasets required to calculate the power factor ($PF = S^2\,\sigma$) and the dimensionless thermoelectric figure of merit ($ZT = S^2\,\sigma\,T/\kappa$) are not always available, and reported data are often limited to partial indicators such as apparent S or effective σ. The absence of unified testing standards remains a major challenge for quantitative comparison across different studies. Meaningful comparison requires

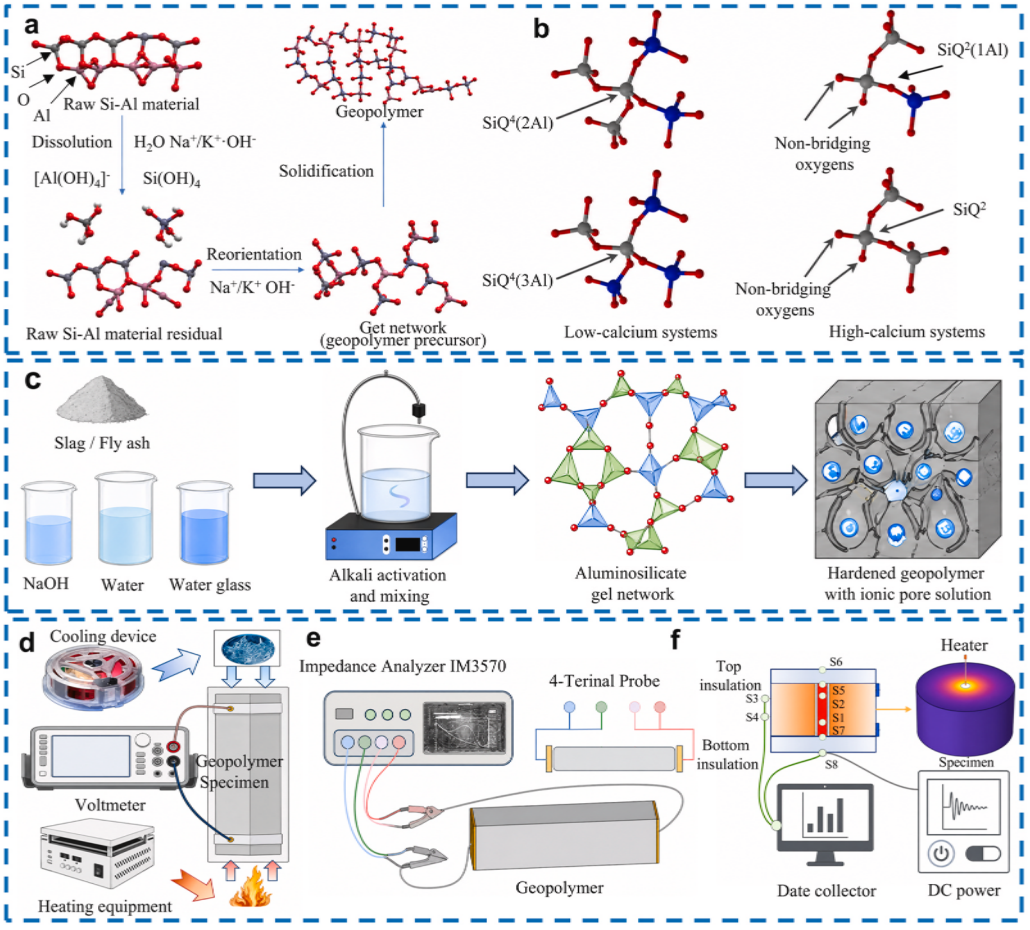


Fig. 2. Formation, processing, and thermoelectric characterization of geopolymer-based systems. (a) Geopolymerization process, reproduced from Ref. [38], Copyright © 2024, with permission from Elsevier. (b) Silicon coordination environments in low- and high-calcium aluminosilicate networks, reproduced from Ref. [39], Copyright © 2022, with permission from Elsevier. (c) Alkali activation, gel formation, and hardening of geopolymer specimens. (d-f) Apparent Seebeck coefficient, effective electrical conductivity, and thermal conductivity measurements, reproduced from Ref. [40], Copyright © 2025, with permission from John Wiley and Sons.

consistent reporting of specimen geometry, moisture state, electrode configuration, temperature-gradient protocol, stabilization criterion, and the methods used to determine S, σ, and κ. Without such information, differences among reported values may reflect testing conditions and boundary effects as much as intrinsic material performance.

2.4. Reported performance levels and emerging trends

Across the available literature, many geopolymer-based systems show measurable thermoelectric responses that are stronger than those typically reported for ordinary cement-based matrices [56,57]. As summarized in Table 1, metakaolin- and kaolin-based systems often exhibit absolute apparent S values exceeding 10^3 μV K^{-1}, suggesting that alkali-activated aluminosilicate frameworks provide an ion-rich environment for thermoelectric voltage generation [58,59]. However, these values should not be read as a direct ranking of thermoelectric efficiency. In several studies, S is reported without corresponding σ and κ data, and the temperature used for ZT calculation is not always specified, which makes PF and ZT difficult to compare on the same basis.

Although Table 1 is organized by precursor type, its main implication is mechanistic rather than taxonomic. Rather than indicating a single optimization pathway, the grouped data reveal a separation of transport regimes. Ion-rich binders tend to produce large apparent S, whereas continuous carbonaceous fillers mainly increase σ and PF by introducing electronic pathways. For example, systems containing carbon nanotube fibers (CNTFs) in metakaolin-based geopolymer matrices show S values of only several tens of μV K^{-1}, but their σ and PF are much higher than those of most ion-dominated geopolymer binders [61,62]. The relatively high κ values reported for these systems, 12.5 and 12.0 W m^{-1} K^{-1}, also require a different interpretation from those of bulk geopolymer matrices, because they were derived from literature thermal-conductivity values of pure or pristine CNTFs for ZT estimation rather than from direct measurements of the geopolymer composite matrix.

The graphite-modified metamorphic shale system further shows how data treatment can affect interpretation [65]. The reported S of 34, 300 μV K^{-1} was obtained for a metashale geopolymer mortar containing 5 wt% graphite powder. This value was calculated from the local derivative of a polynomial voltage-temperature fitting curve near $\Delta T \approx 6$ °C, not from a linear slope over the full temperature-gradient range. The value therefore reflects a protocol-dependent apparent Seebeck coefficient and does not establish a universal graphite-addition effect in geopolymer systems. Because independent replication under standardized humidity, electrode, and temperature-gradient conditions has not yet been established, it is best described as a protocol-sensitive data point, not a reproducible benchmark for graphite-modified geopolymer systems.

For fly ash/slag-based alkali-activated systems, the reported properties are more dispersed because the binders differ in gel chemistry, soluble ion content, water retention, filler connectivity, and electrode contact [68,71]. Some formulations mainly enhance apparent S, whereas others improve σ or modify κ. This diversity confirms that

Table 1
Reported thermoelectric performance of geopolymer-based materials.

Precursor	Activator	Additive	S (μV K^{-1})	σ (S cm^{-1})	κ (W m^{-1} K^{-1})	PF (μW m^{-1} K^{-2})	T_{ZT} (K)	ZT	Ref.
Metakaolin/kaolin-based systems									
Kaolin	NaOH + Na_2SiO_3	–	− 182	5×10^{-5}	0.69	1.66×10^{-4}	323	7.76×10^{-8}	[57]
Metakaolin	NaOH + Na_2SiO_3	–	+ 1736	1.41×10^{-5}	0.20	4.25×10^{-3}	298	6.3×10^{-6}	[28]
Metakaolin	NaOH + Na_2SiO_3	–	+ 7750	–	–	–	–	–	[56]
Metakaolin	NaOH + Na_2SiO_3	MnO_2	− 4273	–	–	–	–	–	[58]
Metakaolin	NaOH + Na_2SiO_3	Fe_2O_3–GNPs	− 1092	7.04×10^{-3}	–	0.84	–	–	[40]
Metakaolin	NaOH + Na_2SiO_3	Glass beads	+ 1240	1.64×10^{-4}	0.488	0.0252	298	1.5 4× 10^{-5}	[59]
Metakaolin	NaOH + Na_2SiO_3	Metallic electrodes	+ 2010	–	–	–	–	–	[60]
Metakaolin	Potassium silicate	CNTFs	+ 45.2	1.64×10^{3}	12.5	335.8	298	8.01×10^{-3}	[61]
Metakaolin	Potassium silicate	CNTFs	+ 47.8	6.74×10^{3}	12.0	1539.1	298	3.82×10^{-2}	[62]
Metakaolin-containing hybrid systems									
Metakaolin + FA	KOH + Na_2SiO_3	–	+ 15.12	–	–	–	–	–	[24]
Metakaolin + FA	KOH + Na_2SiO_3	SiC	+ 29.34	–	–	–	–	–	[52]
Metakaolin + Slag	NaOH + Na_2SiO_3	–	− 2760	1.45×10^{-5}	0.320	1.10×10^{-2}	298	1.03×10^{-5}	[63]
Metakaolin + Slag	KOH + Potassium silicate	Graphite	+ 69.78	1.96×10^{-4}	1.10	9.6×10^{-5}	298	2.6×10^{-8}	[64]
Metamorphic shale-based systems									
Metamorphic shale	KOH + Potassium silicate	CFs	+ 88.7	4.33×10^{-7}	1.13	3.41×10^{-7}	296	8.94×10^{-11}	[53]
Metamorphic shale	KOH + Potassium silicate	Graphite	+ 538	2.23×10^{-8}	0.86	6.46×10^{-7}	298	2.24×10^{-10}	[29]
Metamorphic shale	KOH + Potassium silicate	Graphite	+ 34300	9.76×10^{-5}	0.97	11.48	298	3.54×10^{-3}	[65]
Metamorphic shale	KOH + Potassium silicate	Graphite	+ 14.72	–	–	–	–	–	[66]
Fly ash/slag-based alkali-activated systems									
FA + GGBS	Sodium disilicate + water	SWCNTs– surfactant	+ 15.8	16.6	–	0.414	–	–	[67]
FA + GGBS	Water	MnO_2–PVA	− 5470	2.74×10^{-5}	0.79	8.2×10^{-2}	293	3.0 4× 10^{-5}	[68]
FA + GGBS + OPC	Alkali wastewater (red mud)	Copper slag aggregate	+ 570	8.6×10^{-6}	0.58	2.79×10^{-4}	353	1.7×10^{-7}	[69]
FA + GGBS + RM	NaOH + Na_2SiO_3	ZnO–PVA	− 19.8	4.02×10^{-3}	0.734	1.58×10^{-4}	298	6.4×10^{-8}	[54]
FA + GGBS	NaOH + Na_2SiO_3	–	+ 1353	–	–	–	–	–	[70]
FA + GGBS	NaOH + Na_2SiO_3	MWCNTs	+ 22.63	9.37×10^{-2}	–	4.8×10^{-3}	–	–	[71]
FA + Slag	NaOH + Na_2SiO_3	–	− 1450	2.87×10^{-3}	–	0.60	–	–	[49]
SF + GGBS	NaOH + Na_2SiO_3	CFs−Steel fibers	+ 732.7	2.4×10^{-3}	0.44	0.13	298	8.7×10^{-5}	[55]

Notes: S, apparent Seebeck coefficient; σ, electrical conductivity; κ, thermal conductivity; PF, power factor ($PF = S^2\sigma$); ZT, dimensionless thermoelectric figure of merit; T_{ZT}, absolute temperature used for ZT calculation. The sign of S follows the convention $S = -\Delta V/\Delta T$, where $\Delta V = V_{hot} - V_{cold}$ and $\Delta T = T_{hot} - T_{cold}$. An en dash (–) indicates that the parameter was not reported or measured in the original study. PF and ZT were recalculated from the reported S, σ, κ, and T_{ZT} values when sufficient data were available. Because different studies used different testing setups, specimen geometries, electrode configurations, moisture states, and thermal boundary conditions, the listed values should be compared with caution. Abbreviations: FA, fly ash; GGBS, ground granulated blast-furnace slag; OPC, ordinary Portland cement; RM, red mud; SF, silica fume; CFs, carbon fibers; CNTFs, carbon nanotube fibers; MWCNTs, multi-walled carbon nanotubes; SWCNTs, single-walled carbon nanotubes; GNPs, graphene nanoplatelets; SiC, silicon carbide.

geopolymer thermoelectrics should be discussed as coupled ionic/electronic and thermal transport systems, rather than as a uniform material class. The wide spread of ZT values in Table 1 therefore reflects not only material performance, but also differences in moisture state, electrode configuration, κ determination, fitting method, and reporting completeness [67].

Overall, Table 1 is intended to show that geopolymer-based thermoelectrics currently follow divergent transport regimes, not to rank thermoelectric efficiency. The main trend is not a monotonic improvement in ZT, but a separation between ion-dominated high-S systems, electronically percolated high-σ/PF composites, and protocol-sensitive data points.

3. Binder-level mechanisms governing thermoelectric behavior

Thermoelectric behavior in geopolymer matrices is associated with coupled transport processes within a heterogeneous, ion-containing aluminosilicate binder [40]. As schematically illustrated in Fig. 3, ion-rich geopolymer binders are primarily associated with ionic thermodiffusion and pore-solution redistribution, whereas carbon-modified geopolymers can introduce additional electronic pathways and filler-matrix interfacial polarization [55]. These processes are strongly affected by the amorphous aluminosilicate framework, mobile alkali ions, pore solution chemistry, moisture state, and conductive or interfacial phases [49]. This section synthesizes the current mechanistic understanding of how these binder-level features regulate the thermoelectric response of geopolymer-based systems.

3.1. Amorphous aluminosilicate networks and transport regulation

At the structural level, geopolymers consist of three-dimensional amorphous networks formed by the polycondensation of [SiO_4] and [AlO_4] tetrahedra, with charge balance provided by alkali cations such as sodium or potassium [32,72]. This negatively charged aluminosilicate framework provides a continuous structural environment that can influence the distribution, confinement, and migration of mobile ions within the matrix. Therefore, the geopolymer gel phase should not be regarded as an inert solid phase. Instead, it can interact with

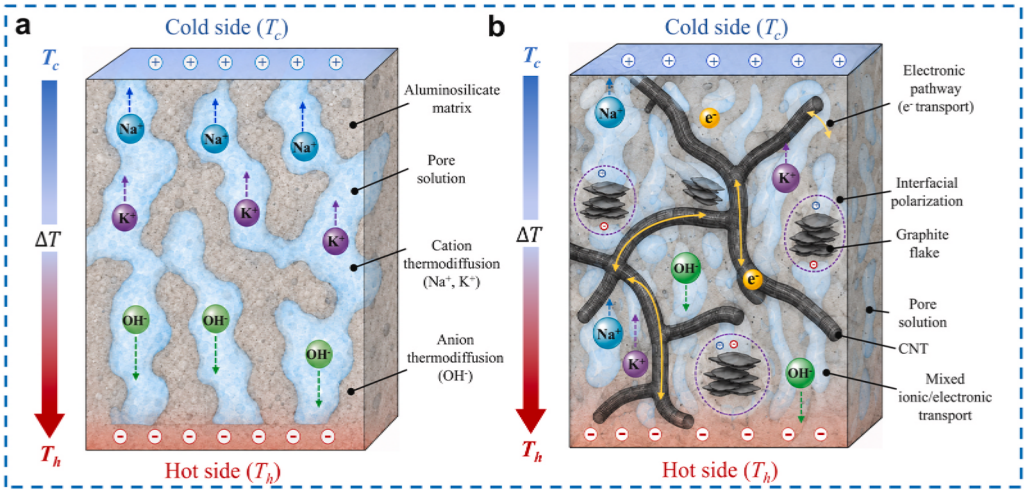


Fig. 3. Thermoelectric transport processes in geopolymer-based systems: (a) ion-rich geopolymer binder in which ionic thermodiffusion, pore-solution redistribution, and electrode boundary effects contribute to the apparent thermovoltage, and (b) carbon-modified geopolymer involving ion-dominated mixed ionic/electronic transport and filler-matrix interfacial polarization.

pore-solution species through electrostatic attraction, surface association, and hydration-related effects [25,73].

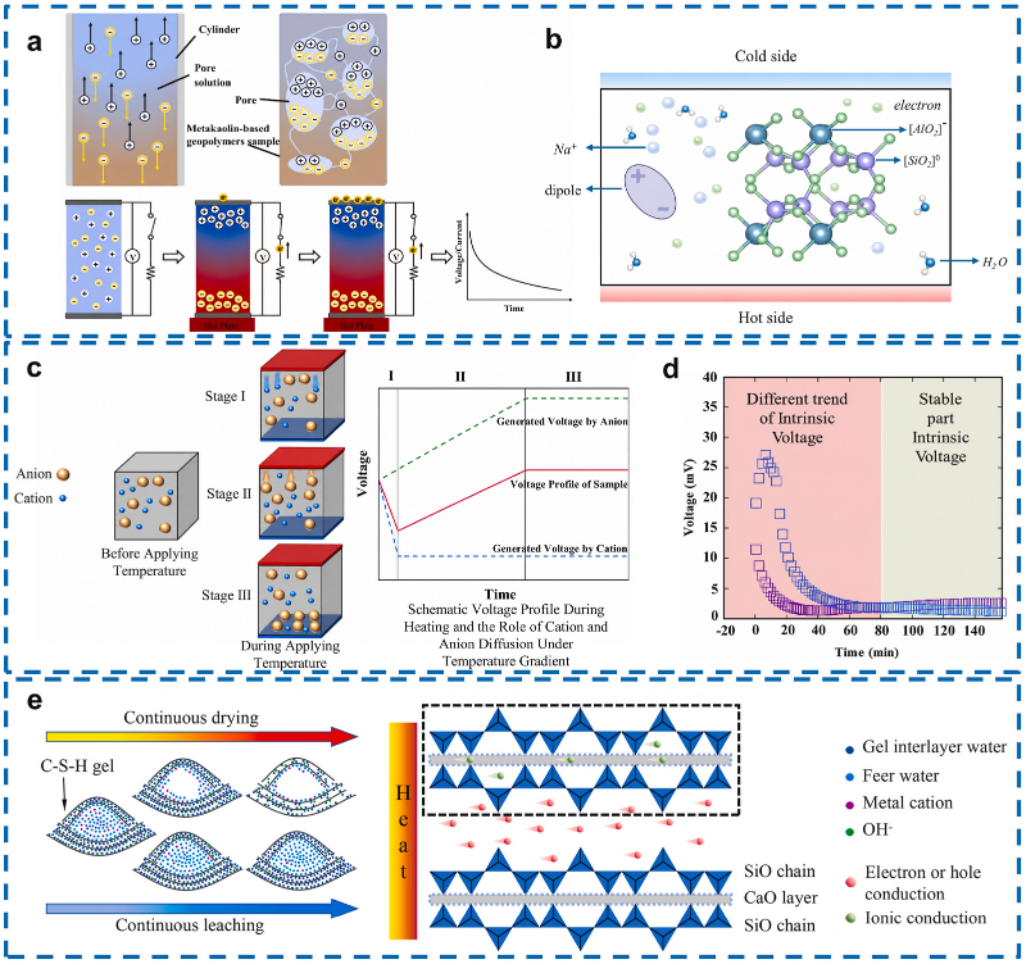


Fig. 4. Experimental and mechanistic evidence for ion-, pore-solution-, and moisture-influenced apparent thermoelectric behavior in geopolymer and alkali-activated binder systems. (a) Pore-solution ion transport and time-dependent voltage response, reproduced from Ref. [56], Copyright © 2025, with permission from Elsevier. (b) Ion redistribution and dipole formation under a temperature gradient, reproduced from Ref. [40], Copyright © 2025, with permission from John Wiley and Sons. (c,d) Cation/anion thermodiffusion, thermovoltage evolution during heating, and transient/quasi-stable voltage regions, reproduced from Ref. [69], Copyright © 2024, with permission from Elsevier. (e) Moisture evolution during drying/leaching and coupled ion/electron transport in gel structures, reproduced from Ref. [49], Copyright © 2025, with permission from Elsevier.

Mobile alkali cations may be associated with negatively charged aluminosilicate sites, while their mobility is further affected by temperature, hydration state, pore-solution chemistry, and pore connectivity [74–76]. Under a temperature gradient, the coupling between framework charge, pore solution, and mobile ions can produce asymmetric ion redistribution and an apparent thermovoltage across the specimen, as schematically shown in Fig. 3a. In this process, the aluminosilicate framework acts not only as a structural skeleton but also as a regulator of ion availability and transport pathways [56].

The importance of framework structure is further supported by comparisons between geopolymer and ordinary cementitious binders. In hydrated cement systems dominated by calcium-silicate-hydrate phases, ion transport may be limited by phase heterogeneity, pore blocking, and discontinuous transport pathways [77]. By contrast, many geopolymer matrices contain more continuous aluminosilicate networks and ion-containing pore solutions, which may support more effective thermally driven ion transport [78]. This structural feature helps explain why geopolymer-based systems often exhibit stronger apparent thermoelectric responses than ordinary Portland cement-based matrices. It also provides the basis for understanding the coupled variations in apparent Seebeck coefficient, electrical conductivity, and thermal conductivity discussed in later sections.

3.2. Role of alkali ions, pore solution, and pore architecture

Available studies indicate that mobile ions in the pore solution make a major contribution to the thermoelectric response of geopolymer binders. Direct measurements reported by Jeon et al. [56] showed that the apparent Seebeck coefficient of the extracted pore solution can be substantially higher than that of the corresponding hardened metakaolin-based geopolymer matrix (Fig. 4a). This observation suggests that pore-solution chemistry and electrode-electrolyte boundary conditions play important roles in translating internal ion redistribution into measurable thermovoltage. In solid specimens, the measured voltage is further influenced by how effectively the pore network maintains continuous ion-transport pathways between the hot and cold ends [49].

Pore architecture also modulates this process. Liang et al. tuned the pore structure of metakaolin-based geopolymers by inert glass bead doping and showed that thermoelectric performance is influenced more strongly by nanoscale pore features and pore connectivity than by total porosity alone. In particular, mesopores in the tens-of-nanometres range were reported to be favorable for ionic thermoelectric behavior, possibly because they provide confined environments for electric-double-layer-related ion redistribution while retaining sufficient connectivity for macroscopic ion transport. However, this finding does not establish a universal optimum pore size for all geopolymer systems. Excessive confinement or poorly connected pores may restrict ion mobility and reduce effective charge transport, indicating that pore-size optimization is subject to a balance between ion selectivity and transport continuity [59,69].

Moisture state is another key factor. Several studies report that drying suppresses thermovoltage and electrical conductivity, while re-wetting can partially or substantially restore the response, reflecting moisture-dependent changes in pore-solution continuity, ion mobility, and gel structure (Fig. 4e) [49,64]. These observations are not readily explained by purely electronic transport alone and support the view that aqueous ion-transport pathways are important for effective thermoelectric operation in many geopolymer and alkali-activated binder systems. Nevertheless, high ion concentration alone is not sufficient; specimens with concentrated but poorly connected pore solution may still show reduced thermoelectric output.

Under an imposed temperature gradient, mobile ionic species can undergo thermodiffusion, leading to spatially non-uniform redistribution of cations and anions (Fig. 4b and c) [79,80]. The resulting electrochemical potential difference can generate a measurable thermovoltage across the electrodes and may produce time-dependent voltage evolution, including transient and more stable regions (Fig. 4d). The magnitude and polarity of the measured response depend on the relative thermal mobility, concentration, and boundary interactions of the dominant ionic species. This mechanism may help explain the polarity reversals and non-linear voltage evolution reported in kaolin-based alkali-activated systems [57].

Overall, these studies suggest that the thermoelectric response of geopolymer binders is not governed by ion concentration alone, but by the combined effects of pore-solution chemistry, pore connectivity, moisture state, and ion-matrix interactions under a temperature gradient.

3.3. Coexistence of ionic and electronic conduction

While ionic transport often makes a major contribution to the thermoelectric response of many reported unmodified geopolymer matrices, electronic conduction is not entirely absent. Hall-effect measurements and conductivity analyses have suggested the presence of electronic charge carriers in some geopolymer matrices, particularly in metakaolin-based systems [56]. However, in ion-containing and moisture-sensitive binders, the measured thermovoltage may include both electronic and ionic contributions, with the ionic component being much larger under many reported conditions [40].

This coexistence of ionic and electronic conduction has led to apparent contradictions in early interpretations [81]. For example, some systems exhibit n-type electronic behavior according to Hall measurements while simultaneously displaying a positive apparent Seebeck coefficient under the adopted voltage convention. Such discrepancies can be rationalized by considering that the measured thermoelectric voltage may be strongly influenced by ionic thermodiffusion, pore-solution redistribution, and electrode boundary effects, while electronic carrier transport contributes in parallel [57,69]. In composite systems deliberately incorporating conductive fillers such as carbon nanotubes and graphite, or interfacially active additives such as MnO_2, electronic or mixed charge-transport pathways can become more prominent, resulting in mixed ionic/electronic transport behavior (Fig. 3b) [58,61]. Even in these cases, however, ionic contributions may remain important, particularly under humid or partially saturated conditions [29,64].

Another characteristic feature of ion-influenced systems is time-dependent voltage evolution. Several studies have reported transient thermoelectric voltage behavior, including initial peaks followed by gradual stabilization or decay, which is consistent with slow ion redistribution, electrode polarization, and interfacial polarization processes [57,60]. Such behavior is not readily explained by purely electronic steady-state transport alone and further indicates the involvement of ion redistribution and interfacial processes. Electrode interfaces therefore act as active boundary regions that influence how internal ion gradients are converted into measurable electrical signals, not merely as passive contacts [56]. These observations also indicate that mixed ionic/electronic transport may affect signal stability during repeated or prolonged measurements. At present, however, irreversible ion depletion or electrochemical degradation has not been directly established as a general degradation mechanism in geopolymer thermoelectric systems. Further long-duration testing, impedance analysis [82,83], and post-exposure chemical characterization are needed to determine whether the observed voltage drift mainly reflects reversible polarization, gradual ion redistribution, or irreversible material changes.

Overall, geopolymer matrices exhibit an ion-dominated mixed transport regime, in which electronic conduction can contribute in parallel depending on matrix composition, filler connectivity, and moisture state. Ionic thermodiffusion, shaped by the amorphous aluminosilicate framework and connected pore network, helps explain the relatively large apparent Seebeck coefficients, polarity variations, strong moisture sensitivity, time-dependent voltage response, and methodological variability reported across the literature.

4. Performance regulation and coupled optimization of thermoelectric properties

Thermoelectric performance is commonly described using the dimensionless figure of merit,

$$ZT = \frac{S^2 \sigma T}{\kappa} \quad (1)$$

although its interpretation as a direct efficiency metric is limited in moisture-dependent, ion-conducting geopolymer systems. Here S is the apparent Seebeck coefficient, σ is the effective electrical conductivity that may include both ionic and electronic contributions, κ is the thermal conductivity, and T is the absolute temperature. The ZT parameter nevertheless remains useful as a comparative descriptor because it reflects the coupling among electrical transport, thermal transport, and thermopower in thermoelectric materials [84]. For geopolymer-based thermoelectrics, parameter optimization is particularly challenging because S, σ, and κ are all affected by pore structure, moisture state, ion distribution, and filler connectivity [57,70]. This coupling makes independent optimization more difficult than in dense electronic thermoelectric solids and requires strategies that balance, rather than separately maximize, the parameters in Eq. (1).

In this section, reported performance-enhancement strategies are reviewed from the perspective of their effects on the three governing parameters in Eq. (1): apparent Seebeck coefficient, effective electrical conductivity, and thermal conductivity. Emphasis is placed on clarifying how these strategies modify transport pathways and why improvements in one parameter may compromise another in geopolymer-based systems.

4.1. Strategies for enhancing electrical conductivity

Improving electrical conductivity has been widely explored in geopolymer-based thermoelectrics, primarily because the intrinsic conductivity of unmodified geopolymer matrices is low [85,86]. In practice, charge transport often involves the coexistence of electronic conduction through conductive fillers and ionic migration within the geopolymer pore network (Fig. 5a). Reported approaches can be broadly classified into electronic pathway engineering and ionic-transport facilitation.

4.1.1. Electronic pathway engineering via conductive fillers

The most direct route to increasing σ involves incorporating electronically conductive fillers or interfacially active additives, as reported for MnO_2-modified and carbon-reinforced geopolymer matrices. These additives can provide additional electronic, interfacial, or mixed charge-transport pathways within the relatively low-conductivity aluminosilicate matrix (Fig. 5a–f) [58,88,90]. For carbon-based systems, increasing filler content can promote pathway continuity and eventually form a percolated conductive network (Fig. 5b).

In geopolymer matrices, reported percolation behavior appears to depend on filler type, dispersion state, aspect ratio, filler-matrix interaction, and the connectivity of the pore/binder network. Conductive fillers may reach an apparent percolation threshold at comparable or, in some cases, slightly lower volume fractions than those reported for ordinary Portland cement-based composites, although direct comparison remains difficult because filler geometry, dispersion method, matrix chemistry, and threshold definition vary among studies [91,92]. Once a continuous conductive network is established, electrical conductivity

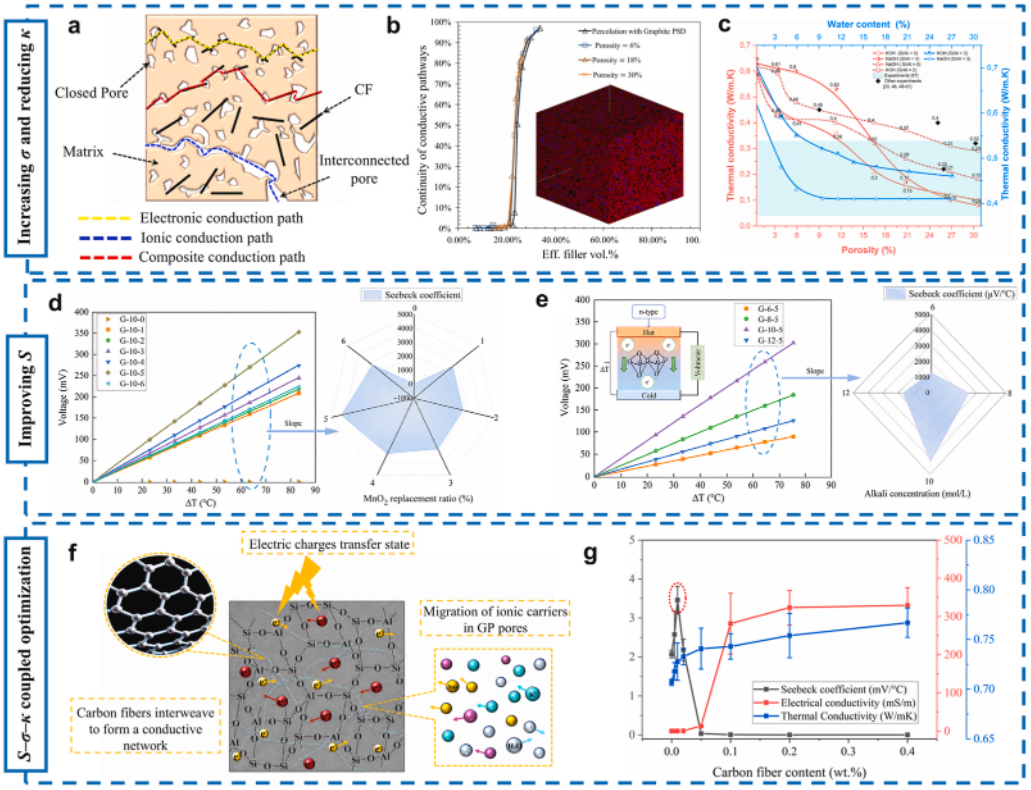


Fig. 5. Performance-enhancement strategies and coupled parameter responses in geopolymer-based thermoelectric systems. (a) Electronic, ionic, and mixed conduction pathways in porous geopolymer composites, reproduced from Ref. [70], Copyright © 2025, with permission from Elsevier. (b) Conductive-filler percolation and pathway continuity, reproduced from Ref. [86], Copyright © 2024, with permission from Elsevier. (c) Thermal-conductivity regulation by porosity and water content, reproduced from Ref. [87], Copyright © 2023, with permission from Elsevier. (d,e) Apparent Seebeck coefficient regulation by functional additives and alkali concentration, reproduced from Ref. [58], Copyright © 2023, with permission from John Wiley and Sons. (f) Carbon-fiber-assisted charge transfer and ionic-carrier migration, reproduced from Ref. [88], Copyright © 2024, with permission from Elsevier. (g) Coupled variations in apparent Seebeck coefficient, effective electrical conductivity, and thermal conductivity with carbon-fiber content, reproduced from Ref. [89], Copyright © 2026, with permission from Elsevier.

can increase by several orders of magnitude, corresponding to the formation of long-range electronic pathways near or above the percolation threshold (Fig. 5b) [86,93].

However, from a thermoelectric standpoint, conductivity enhancement via electronic fillers introduces potential trade-offs. First, increasing σ through electronic pathways may reduce the measured apparent Seebeck coefficient, showing a trade-off that is qualitatively analogous to carrier-concentration effects discussed in semiconductor thermoelectrics [55,94]. Second, highly connected electronic networks may provide parallel electronic transport pathways that partially mask or weaken the relative contribution of ion-mediated thermovoltage [95]. Conductive fillers should be evaluated not only by their ability to increase σ, but also by their effects on S, κ, moisture retention, interfacial stability, and the balance between ionic and electronic transport.

Conductivity enhancement through fillers must also be considered together with processing and mechanical performance [68]. A filler content that promotes electronic pathway formation may not be compatible with workability, uniform dispersion, or strength retention, especially for high-aspect-ratio or nanoscale carbon fillers. Practical filler design should aim for useful electrical connectivity at the lowest effective dosage while preserving mixability, pore-solution continuity, moisture stability, and mechanical performance [86]. These constraints become especially relevant when geopolymer thermoelectrics are considered for construction-compatible applications.

4.1.2. Ionic conductivity enhancement and its limits

An alternative approach focuses on enhancing ionic conductivity by increasing alkali ion availability or improving pore connectivity [96,97]. Higher ionic mobility can increase effective charge transport, particularly in partially saturated systems. However, ionic conductivity enhancement is closely linked to moisture state, making the response sensitive to drying, temperature fluctuations, and long-term ion redistribution [28,93].

Unlike electronic conductivity in a continuous percolation network, ionic conductivity does not necessarily scale linearly with ion concentration once pore connectivity, ion-ion interactions, electrostatic screening, and framework binding are considered. Excessive alkali content may reduce effective ion mobility or decrease response stability through ion pairing, stronger ion-matrix association, or changes in pore-solution chemistry [98–100]. Increasing ion concentration alone is unlikely to provide a robust route for improving thermoelectric performance unless pore-solution continuity and moisture stability are also maintained.

4.2. Strategies for reducing thermal conductivity

Reducing thermal conductivity is a central strategy for improving the apparent ZT value and maintaining a useful temperature gradient. Geopolymer matrices already exhibit relatively low κ values compared with dense inorganic solids, and further suppression of heat transport has been pursued through microstructural and compositional engineering [101].

4.2.1. Porosity engineering and heat-path interruption

Thermal transport in geopolymers is mainly associated with heat transfer through the solid skeleton, pore solution, and gas-filled pores [102]. Increasing porosity and pore tortuosity can interrupt continuous heat-conduction pathways and reduce κ, as reflected by the coupled effects of porosity and water content shown in Fig. 5c. Such effects can be achieved by tailoring precursor particle packing, curing regimes, or introducing inert or porous fillers [103].

However, reducing κ through porosity engineering is not automatically beneficial for thermoelectric performance. In geopolymer systems, the pore network also governs moisture retention and ion migration. Excessive or poorly connected porosity can lower κ but simultaneously disrupt ionic continuity, reduce mechanical integrity, or accelerate drying, leading to competing effects on ZT [104]. This trade-off is different from that commonly discussed in crystalline thermoelectrics, where phonon scattering can sometimes be enhanced without strongly disturbing electronic transport. Pore design should reduce heat transfer without disrupting water-filled ion-transport pathways or mechanical continuity.

4.2.2. Low-thermal-conductivity fillers and hierarchical structures

The incorporation of lightweight or low-κ fillers, such as hollow particles or porous inclusions, has also been explored. These strategies aim to reduce heat transfer through the solid skeleton while preserving sufficient pathways for charge transport. Hierarchical pore structures combining micro-, meso-, and macropores have been proposed as a possible route to lower κ while maintaining ion transport pathways [105–107].

In geopolymer thermoelectrics, the realistic objective is not complete decoupling of thermal and ionic transport, because both are affected by pore structure and moisture state. Instead, partial separation of heat-transfer and ion-transport pathways may be pursued through controlled pore and filler design. Hierarchical pore structures may interrupt continuous solid heat-transfer paths while retaining connected, water-filled pores for ion migration. Compatible lightweight or low-κ inclusions may reduce the effective thermal conductivity of the solid skeleton, provided that they do not excessively dilute the ion-conducting binder phase or create poorly connected pores [104]. Moisture-retaining or ion-buffering phases may also be explored as future strategies to preserve pore-solution continuity when thermal-insulation design increases drying sensitivity [108]. The key constraint is that pores or inclusions introduced for thermal insulation should not isolate the liquid-filled pathways that carry mobile ions.

Nevertheless, the effectiveness of such strategies remains highly system-dependent. Mechanical degradation, moisture sensitivity, and long-term structural stability remain key concerns, particularly for construction-compatible applications [109]. κ reduction should be evaluated together with strength retention, moisture stability, and electrical output rather than as an isolated target.

4.3. Strategies for enhancing the apparent Seebeck coefficient

Enhancing the apparent Seebeck coefficient in geopolymer systems follows a different logic from that used in conventional semiconductor thermoelectrics. In many geopolymer-based systems, the measured S represents an apparent response associated with ionic thermodiffusion, pore-solution redistribution, and interfacial processes, and it cannot be explained solely by electronic energy filtering or band-structure engineering [56,110].

4.3.1. Ion species, concentration, and thermodiffusion

Reported studies indicate that the magnitude and polarity of S depend strongly on alkali ion species, ion concentration, and hydration state [49]. Differences between sodium- and potassium-activated binders are generally discussed in relation to ion size, hydration energy, and mobility. Adjusting activator chemistry and precursor composition can therefore modulate S without necessarily introducing conductive fillers (Fig. 5e) [111].

Functional additives may also influence S by modifying ion distribution, local interfacial environments, or redox-active sites, as reflected in the reported changes in apparent Seebeck coefficient with MnO_2 replacement ratio (Fig. 5d) [58]. However, large apparent Seebeck coefficients achieved through ion-mediated mechanisms are often accompanied by slow response, time-dependent voltage evolution, and sensitivity to boundary conditions. These features complicate direct comparison with electronic thermoelectrics and the use of conventional steady-state thermopower definitions [56].

4.3.2. Framework-ion interactions and confinement effects

Interactions between mobile ions and the negatively charged aluminosilicate framework can influence S by affecting ion availability, mobility, and thermally driven redistribution. Mesoporous confinement may further promote ion separation associated with electric double layers and support selective ion transport, as discussed in Section 3.2 [59,64]. From a design perspective, enhancing S therefore requires a balance among ion concentration, pore confinement, pathway connectivity, and moisture retention, instead of simply increasing the amount of mobile ions.

4.4. Coupling, trade-offs, and theoretical considerations for ZT optimization

A central challenge in geopolymer-based thermoelectrics is the strong coupling among S, σ, and κ. Strategies that improve one parameter often compromise another, because heat and charge transport are both influenced by pore structure, moisture state, ion distribution, and filler connectivity within the geopolymer matrix. As a result, the transport parameters are interdependent and difficult to decouple through conventional optimization approaches [30].

In classical thermoelectric theory, decoupling strategies aim to suppress heat transport without compromising charge mobility. The phonon-glass electron-crystal concept provides a useful analogy for this decoupling objective, but it should not be treated as a direct materials analogue for geopolymer systems [112]. In geopolymer systems, a comparable goal would be to suppress heat conduction while preserving ion-mediated thermovoltage generation and sufficient electrical conductivity. However, because heat transfer, ion migration, and moisture retention are all linked to the pore network, such decoupling is difficult to achieve in practice [79,113].

The coupled response shown in Fig. 5g illustrates this challenge: changes in carbon-fiber content can modify the apparent Seebeck coefficient, effective electrical conductivity, and thermal conductivity simultaneously, rather than improving each parameter independently [89]. Therefore, conventional band-structure-based optimization frameworks are not directly transferable to amorphous, ion-conducting geopolymer systems. More suitable theoretical descriptions that combine thermodiffusion, electrochemical potential gradients, porous transport, and interfacial effects would help interpret coupled transport behavior and guide more reliable performance-oriented design [114].

Overall, improving thermoelectric performance in geopolymers depends on balancing competing transport processes rather than optimizing each parameter separately. This view highlights the need to move beyond isolated material-level optimization toward integrated design strategies that consider transport physics, environmental stability, mechanical compatibility, and device integration jointly [70].

5. From geopolymer thermoelectric binders to infrastructure-integrated devices

Because the measured response of geopolymer thermoelectric binders is closely linked to moisture state, pore connectivity, and electrode interfaces, device performance cannot be inferred from material-level S, σ, and κ alone [56]. Device development calls for element-level design, interface control, moisture-regulated packaging, durability validation, and application-oriented reporting [71].

For construction environments, the relevant question is not only whether a geopolymer binder can generate a large apparent Seebeck coefficient, but whether this response can be collected, stabilized, and used under realistic thermal and environmental conditions. Building envelopes, pavements, tunnels, and industrial surroundings provide small and fluctuating temperature gradients. These conditions are more suitable for local signal generation, intermittent energy harvesting, and low-power sensing than for sustained high-power generation. In such settings, device design should prioritize electrode stability, moisture-regulated packaging, durability under environmental cycling, and compatibility with construction processes [7].

5.1. Device demonstrations and current maturity level

Table 2 summarizes representative device-related demonstrations and functional outputs reported for geopolymer and related alkali-activated thermoelectric systems. Taken together, these studies show that the field has progressed from material-level thermovoltage measurements toward device-like demonstrations, but most reported systems remain at the proof-of-concept or element level. Representative device configurations and output demonstrations are further illustrated in Fig. 6 [62].

The reported demonstrations mainly follow two directions. The first is sensing-oriented validation [68], where geopolymer thermoelectric elements are used to detect temperature gradients, mechanical damage, or environmental changes through voltage response. These studies establish that the thermoelectric response can be translated into a functional signal, although they generally do not demonstrate sustained power delivery. The second direction is output amplification through series connection or module-like assembly [61]. For example, Jeon et al. connected nine metakaolin-based geopolymer cylinders in series and powered a small red LED for 4 s, reaching $V_{out} \approx 2.3$ V under a large imposed temperature difference [56]. This demonstration indicates functional activation, while also showing that the output remains closely tied to element connection and imposed thermal conditions.

The device-level data in Table 2 also show a clear mismatch between measurable output and practical readiness. Reported maximum power values, when available, range from the nanowatt level to the tens-of-microwatt level [67]. Higher outputs are usually associated with multi-element assemblies, larger imposed temperature differences, or controlled laboratory configurations. For instance, Park et al. reported an AAM/MWCNT module that reached the tens-of-microwatt level under a large imposed temperature gradient [71]. This suggests that module assembly can increase measurable output, but service-relevant operation under smaller and fluctuating gradients remains insufficiently demonstrated.

Overall, the key issue is whether the generated signal can be converted into stable, load-compatible, and durable device output. Many studies still emphasize open-circuit voltage, short-term maximum power, or brief functional demonstrations, whereas internal resistance, load matching, response time, humidity condition, electrode stability, and cycling retention are not yet reported in a consistent manner. At present, current device studies provide evidence of functional feasibility and device sensitivity, but not yet of mature energy-harvesting performance [61].

From an application perspective, the evidence in Table 2 points more strongly toward low-power infrastructure functions than toward continuous power generation. Temperature-gradient sensing, event-triggered response, capacitor charging, damage-tolerant signal generation, and auxiliary power for sensor nodes are more realistic near-term targets. Future device studies should shift from demonstrating voltage generation alone to reporting useable output under defined loads, realistic temperature gradients, controlled moisture conditions, and repeated environmental exposure [67].

5.2. Electrode-binder interfaces and signal stability

The electrode-binder interface determines whether an ion-mediated voltage response can be collected as a stable electrical signal. In geopolymer thermoelectrics, this region acts as both an electrical contact and an electrochemical boundary connected to pore solution and mobile alkali ions. During heating, ion accumulation and interfacial polarization may evolve near the electrode, leading to voltage drift, hysteresis, or contact-dependent variation [60,115].

These interface effects are central to interpreting apparent Seebeck

Table 2
Device-related demonstrations and functional outputs of geopolymer-based thermoelectric systems.

System	Device	Configuration	Test condition	Output/function	Ref.
Sensing-oriented validation					
MnO_2-SHGC	TE sensing component	Single sensing specimen	Ambient condition	$P_{out} \approx 0.057$ μW per cylinder; $P_D = 29$ μW m^{-2}; 69% ZT retained after cracking	[68]
p/n CNTF-GP mortar	Temperature sensor	8 p-n thermocouples in series	$\Delta T = 30$ K	$V_{oc} = 7.8$ mV; $P_{max} = 3.1$ nW; stable for 600 s; reversible response to ≈10 °C	[62]
Output-oriented device demonstration					
p/n CNTF-GP concrete	Structural TEG	8 p-n junctions in series	$\Delta T = 50$ K	$V_{oc} = 28.5$ mV; $P_{max} = 0.3$ μW; $P_D = 8$ mW m^{-2}; stable for 5 h	[61]
SWCNT-AAM composite	TEG device	SWCNT-AAM thermoelements	$\Delta T = 60$ K	$V_{oc} \approx 7.5$ mV; $P_{max} = 0.695$ μW; $P_D = 372$ nW m^{-2}; stable for 5 h	[67]
AAM/MWCNT composite	TEG module	130 TE elements	$T_{hot} = 200$ °C; $T_{cold} = 21.6$ °C; $\Delta T = 178.4$ K	$P_{max} = 30.83$ μW; high-temperature harvesting	[71]
Metakaolin-based GP	Series demonstration	9 cylinders in series	$\Delta T \approx 150$ K	$V_{out} \approx 2.3$ V; powered a 3 mm red LED for 4 s	[56]

Notes: TEG, thermoelectric generator; TE, thermoelectric; CNTF, carbon nanotube fiber; GP, geopolymer; MWCNT, multi-walled carbon nanotube; SHGC, strain-hardening geopolymeric composite; SWCNT, single-walled carbon nanotube; AAM, alkali-activated material; p/n, p-type and n-type thermoelements; V_{oc}, open-circuit voltage; V_{out}, output voltage; P_{max}, maximum output power; P_{out}, output power; P_D, power density; ΔT, temperature difference; T_{hot} and T_{cold}, hot-side and cold-side temperatures, respectively. The listed outputs were obtained under different device geometries, temperature gradients, loading conditions, and testing durations.

coefficients obtained from two-electrode measurements. Differences in electrode material, surface preparation, contact pressure, contact area, and testing time may change the measured response without necessarily reflecting a change in binder chemistry. Interface effects are especially relevant when comparing studies that use attached foils, embedded meshes, conductive papers, carbon-based layers, or paste electrodes [116,117].

More reproducible devices require controlled contact architectures, not empirical attachment. Chemically stable electrodes, defined contact geometry, inert conductive interlayers, ion-buffering transition layers, and compliant contacts may help reduce contact variability while maintaining electrical continuity. The practical aim is to stabilize and quantify these interfacial contributions, since they are unlikely to be fully eliminated in ion-conducting binders [115,118].

Interface assessment should combine electrical output with diagnostic measurements. Electrochemical impedance spectroscopy can help distinguish bulk and interfacial resistance contributions, while open-circuit voltage relaxation and chronoamperometry can track slow drift and ion redistribution. Comparisons between blocking and non-blocking electrodes may further clarify electrode polarization and leakage pathways. At minimum, device studies should report electrode material, contact method, contact area, moisture condition, temperature-gradient history, and measurement duration [82,83].

5.3. Packaging, moisture regulation, and durability validation

Packaging in geopolymer thermoelectric devices should focus on moisture regulation instead of simple sealing. Because ion-mediated output depends on sufficient pore-solution continuity, excessive drying can reduce signal output, whereas uncontrolled water ingress or leaching may change ion concentration and interfacial state. A useful package should maintain a moisture window that supports ion transport while limiting environmental degradation [57].

Possible approaches include polymer-inorganic coatings, semi-permeable barriers, multilayer encapsulation, surface treatments around electrodes, and internal water-retaining phases [119,120]. These designs should be evaluated by their ability to stabilize voltage, internal resistance, and mechanical integrity, rather than by moisture loss alone. Overly impermeable encapsulation may restrict exchange but also trap degradation products or introduce thermal and mechanical mismatch. Overly permeable protection may preserve short-term ion transport but fail to limit leaching or external ion exchange [121].

This concern is closely related to the long-term stability of ionic transport pathways in alkali-activated binders. Carbonation can lower pore-solution alkalinity and change carbonate/bicarbonate equilibria, while alkali leaching or efflorescence can remove mobile Na^+ and K^+ species through connected pores [122,123]. The extent and direction of these changes depend on precursor chemistry, calcium content, pore structure, moisture state, and exposure conditions. These processes may modify alkali-ion availability, pore-liquid conductivity, and the continuity of water-filled transport pathways. For geopolymer thermoelectrics, such changes are relevant because ion-mediated signals rely on mobile ions, connected pore solution, and stable electrode-boundary conditions. Therefore, packaging should not only retain an appropriate moisture state, but also limit CO_2 ingress, alkali loss, and external ion exchange when long-term construction use is considered.

Durability validation should be developed together with packaging design. For construction deployment, testing should include repeated thermal gradients, wetting-drying cycles, carbonation or chemical exposure, alkali-leaching or external ion-exchange conditions, and mechanical loading when relevant [122–124]. The purpose is to determine how much output and signal stability remain after service-related exposure, not only to measure the initial apparent Seebeck coefficient or peak power [125].

Useful descriptors include voltage retention after thermal or humidity cycling, drift under a fixed temperature difference, recovery after drying and re-wetting, internal resistance evolution, leachate chemistry or extractable alkali content when leaching exposure is involved, pore-solution composition where feasible, and mechanical retention after functional modification. These parameters would make durability evaluation more closely aligned with device operation in construction environments [126].

5.4. Application windows in construction: low-grade heat harvesting and self-powered sensing

A plausible near-term application window for geopolymer thermoelectrics is local thermal-electrical functionality instead of bulk electricity generation. Temperature gradients in buildings, pavements, tunnels, underground spaces, and industrial surroundings are often modest and fluctuating, but they can still be useful when the task requires a detectable signal or intermittent energy pulse instead of continuous power supply [127].

On this basis, several near-term roles are more realistic than sustained power generation. Geopolymer thermoelectric elements may be used for temperature-gradient sensing, local thermal monitoring,

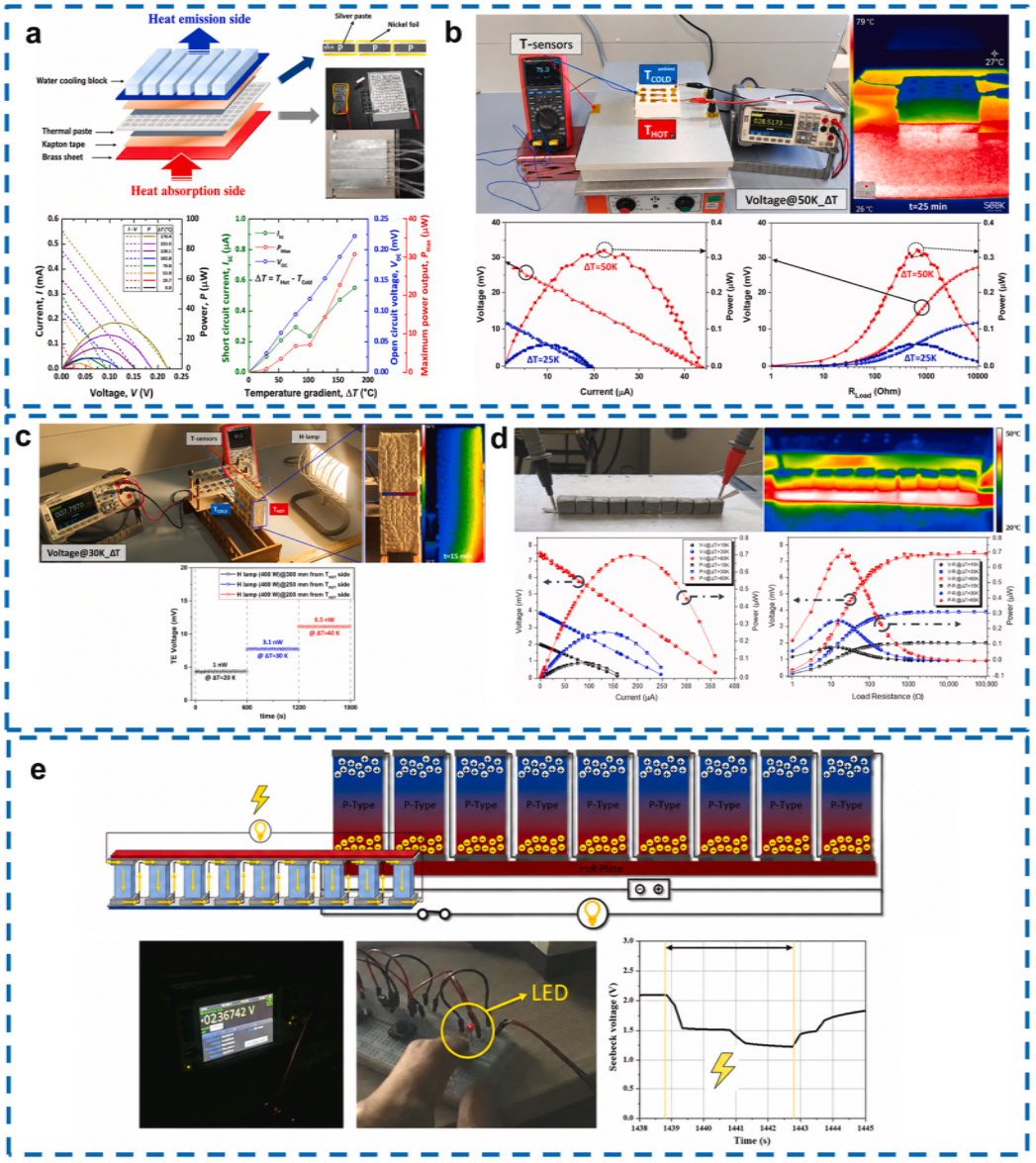


Fig. 6. Representative device-related demonstrations of geopolymer and related alkali-activated thermoelectric systems. (a) AAC/MWCNT module configuration and output variation with temperature gradient, reproduced from Ref. [71], Copyright © 2021, with permission from Elsevier. (b) Device-level voltage and power output under controlled through-thickness temperature differences, reproduced from Ref. [61], Copyright © 2024, with permission from Elsevier. (c) Low-grade heat response under lamp heating, reproduced from Ref. [62], licensed under CC BY 4.0. (d) SWCNT-based TEG device with thermal-field distribution and load-dependent output, reproduced from Ref. [67], licensed under CC BY 4.0. (e) Series-connected metakaolin-based geopolymer elements for short-term LED activation, reproduced from Ref. [56], Copyright © 2025, with permission from Elsevier. These examples illustrate the transition from material-level thermovoltage measurements toward proof-of-concept device demonstrations.

damage-related warning, intermittent capacitor charging, or auxiliary power for low-duty-cycle sensor nodes [68,128]. These tasks can accommodate intermittent output, provided that signal threshold, repeatability, and retention are verified under relevant conditions.

Construction compatibility remains a necessary constraint. For cast-in-place or prefabricated components, conductive fillers, electrodes, encapsulation layers, and water-retaining phases should not severely compromise mixing, curing, shaping, mechanical performance, or long-term durability [129,130]. For surface-attached elements, heat-flow access, contact stability, environmental protection, and maintenance become more important than bulk material optimization alone.

Performance evaluation should start from the intended task. For structural health monitoring, the minimum requirement is not a universal *ZT* or peak power value, but a task-specific output threshold. Relevant questions include the minimum temperature difference needed to produce a readable signal, whether the output remains distinguishable from baseline drift, the response time under a defined load, the time required to charge a small capacitor when intermittent operation is targeted, and the retained function after environmental exposure [67,131]. This task-based view positions geopolymer thermoelectrics as low-power, structure-integrated thermoelectric components rather than replacements for commercial thermoelectric modules.

5.5. *Carbon-footprint and resource considerations for device-level deployment*

Sustainability is an important motivation for developing geopolymer and alkali-activated thermoelectric systems, but it cannot be evaluated only from the low-carbon character of the binder [132]. When thermoelectric function is translated from material specimens to devices, the

material inventory may also include conductive fillers, electrodes, interconnects, auxiliary substrates, encapsulation layers, and processing-related components [133]. These non-binder components can become important, especially when the target application shifts from small laboratory specimens to large-area, structure-integrated sensing or energy-harvesting elements. Therefore, a device-level sustainability discussion requires at least a transparent estimate of material burden, even when complete life-cycle assessment (LCA) data are not yet available.

To provide a bounded quantitative reference, a reported-geometry screening calculation was conducted for representative thermoelectric device demonstrations. The calculation used device geometries, thermoelement dimensions, mixture designs, and component information reported in the cited studies. For geopolymer/AAM and cement-based devices, the values should be interpreted as material-burden screening estimates rather than full module LCAs. Conductive adhesives, wires, tapes, scaffolds, surrounding mortar, encapsulation materials, processing energy, use phase, and end-of-life were excluded when their masses or process inventories were not reported. For Bi_2Te_3-based TEGs, published cradle-to-gate module-level LCA values were used directly rather than recalculated from the material factors in Table 3 [141].

The material-level global warming potential and embodied energy were estimated as:

$$GWP_{case} = \sum_i m_i EF_i$$
$$EE_{case} = \sum_i m_i EI_i \quad (2)$$

where m_i is the mass of material i, EF_i is the embodied-carbon factor, and EI_i is the embodied-energy factor. The areal values were then calculated as:

$$GWP_{areal} = \frac{GWP_{case}}{A}$$
$$EE_{areal} = \frac{EE_{case}}{A} \quad (3)$$

where A is the reported device or module footprint. When a fixed module footprint was not reported, the active thermoelement area was used. These calculations provide material-burden screening estimates rather than functional-unit-based LCA results.

Table 3
Material embodied-carbon and embodied-energy factors used for screening calculations.

Material	Embodied carbon (kg CO_2-eq t^{-1})	Embodied energy (MJ t^{-1})	Ref.
Metakaolin	400	3480	[134]
OPC	912	5500	[135]
FA	4	100	[135]
GGBS	42	200	[135]
Sand/fine aggregate	2.4	80	[135]
Waterglass/sodium silicate solution	1500	5400	[136]
Sodium disilicate Na_2SiO_3 powder	1860	9400	[135]
NaOH	630	3500	[136]
Cu foil	4040	42000	[137]
Expanded graphite/ graphite	13800	45900	[138]
CNTs (SWCNT/MWCNT proxy)	40000	800000	[139]
ZnO	4910	62700	[140]
Water	0.8	10	[135]

Note: The listed factors were used only for the screening calculations in Table 4 and should not be interpreted as harmonized process-resolved LCA data. Cu foil, expanded graphite/graphite, CNTs, and ZnO were treated as proxy or scenario factors where directly comparable device-specific production data were unavailable. The ZnO factor was estimated from primary zinc LCA data according to the Zn mass fraction in ZnO. GWP denotes global warming potential; other abbreviations follow the definitions given in Tables 1 and 2

The results in Table 4 provide an order-of-magnitude reference for the material burden of representative thermoelectric device demonstrations. The published Bi_2Te_3 module-level LCA gives areal GWP values of 499–941 kg CO_2-eq m^{-2} and areal embodied-energy values of 3211–6084 MJ m^{-2}. Under the adopted screening boundary, the mineral-binder cases show lower areal values, with GWP ranging from 5.38 to 35.8 kg CO_2-eq m^{-2} and embodied energy ranging from 70.1 to 190 MJ m^{-2}. This comparison should be interpreted cautiously because the Bi_2Te_3 values are process-resolved module-level LCA results, whereas the geopolymer/AAM and cement-based values are reported-geometry estimates with incomplete auxiliary-component inventories. The results therefore do not establish equivalence in output power, conversion efficiency, operating temperature, service lifetime, or lifetime energy generation.

Within the mineral-binder cases, FA/GGBS-based AAM devices show relatively low screening values. The AAM/MWCNT and SWCNT-AAM TEGs give areal GWP values of 5.38 and 7.55 kg CO_2-eq m^{-2}, which are lower than the cement-based TE module assessed here [67,71]. The CNTF/GP TE sensor also shows a relatively low areal GWP of 9.77 kg CO_2-eq m^{-2}, which is lower than the cement-based reference assessed here [142]. By contrast, the CNTF/GP structural TEG gives a higher areal GWP than the cement-based reference in this screening. These results suggest that the material-burden advantage of geopolymer/AAM systems is not inherent to the binder type alone, but depends on precursor selection, activator dosage, conductive filler content, electrode design, device geometry, and the amount of active material included in the assessed case.

The roles of activators and conductive fillers are particularly important. Sodium silicate solution, sodium disilicate, and NaOH can contribute noticeably to the carbon and energy burden of geopolymer/AAM systems, even when the aluminosilicate precursor is derived from low-burden industrial by-products [136]. Conductive additives and current collectors may also affect the total inventory. In this screening, CNTs, MWCNTs, expanded graphite, Cu foils, and ZnO were included through proxy or scenario factors because production routes and device-specific inventories are rarely reported [139,140,143]. These assumptions do not allow a definitive ranking of device routes, but they indicate that sustainability optimization should consider activator selection, filler dosage, electrode configuration, and auxiliary components, rather than relying only on binder replacement.

Resource considerations further distinguish conventional Bi_2Te_3 modules from mineral-binder thermoelectric devices. Bi_2Te_3-based TEGs rely on tellurium-, bismuth-, antimony-, and selenium-containing thermoelectric materials, together with metallic interconnects, ceramic plates, contact layers, and encapsulation components [141]. Some of these elements are associated with concentrated supply chains, by-product recovery routes, or recycling challenges [141,144]. Large-scale deployment therefore depends not only on module carbon footprint, but also on material availability, supply-chain resilience, and end-of-life recovery. In this context, recycling of thermoelectric legs and recovery of critical elements remain important for conventional Bi_2Te_3-based devices.

Geopolymer and AAM thermoelectric systems provide a different sustainability pathway. Their binder phase can incorporate aluminosilicate-rich industrial by-products such as fly ash and slag, which supports circular use of solid wastes and reduces reliance on primary Portland cement or scarce thermoelectric elements [145]. This pathway is relevant for construction-scale applications, where large surface areas are available and the target function is often low-power sensing, intermittent energy harvesting, or distributed thermal monitoring rather than high-efficiency power generation. However, this potential benefit may be reduced if high activator dosages, large amounts of conductive fillers, or heavy auxiliary components are required [67].

Future studies should report carbon- and energy-burden descriptors

Table 4
Embodied-carbon and energy screening of representative thermoelectric devices.

Assessed system	Components	GWP (kg CO_2-eq $unit^{-1}$)	Areal GWP (kg CO_2-eq m^{-2})	Embodied energy (MJ $unit^{-1}$)	Areal embodied energy (MJ m^{-2})	Ref.
Bi_2Te_3-based TEG	Published full module inventory	0.798–1.506	499–941	5.137–9.735	3211–6084	[141]
Cement-based TE module	Cement, expanded graphite, ZnO	2.21	24.6	11.54	128	[142]
AAM/MWCNT TEG	FA, slag, NaOH, sodium silicate, MWCNT	0.266	5.38	3.80	76.9	[71]
SWCNT-AAM TEG	FA, GGBS, Na_2SiO_3, SWCNT	0.0076	7.55	0.099	99.4	[67]
CNTF/GP TE sensor	CNTF/GP blocks, Cu foils	0.0977	9.77	0.701	70.1	[62]
CNTF/GP structural TEG	GP matrix, Cu foils	0.358	35.8	1.90	190	[61]

Note: Values for mineral-binder systems represent reported-geometry material-burden screening estimates rather than full module LCAs. Components without reported masses or process inventories were excluded. Bi_2Te_3-based TEG values were taken directly from published cradle-to-gate module-level LCA data. Abbreviations follow the definitions given in Tables 1–3.

together with thermoelectric performance descriptors. At minimum, device-level studies should report module footprint, thermoelement dimensions, active material mass, mixture design, electrode and interconnect materials, encapsulation strategy, output under load, operating duration, and post-exposure retention [141,146]. Such information would support more transparent material-burden, resource, and circularity assessment. For geopolymer/AAM thermoelectrics, this reporting is important because their potential value lies not in directly replacing high-efficiency Bi_2Te_3 modules, but in enabling low-material-burden and structure-compatible thermoelectric functions at construction scale.

5.6. Toward application-oriented evaluation and reporting

Geopolymer thermoelectrics need to be evaluated in a way that reflects both ion-mediated transport and structure-integrated use. Conventional indicators such as *ZT* and power factor remain useful when the required parameters are available and measured under comparable conditions, but they are not sufficient on their own for describing moisture-sensitive, ion-conducting, and construction-compatible systems [147]. Device-relevant information should therefore accompany the reported material response.

A useful reporting scheme can connect three levels of information. At the material level, key descriptors include the apparent Seebeck coefficient, effective electrical conductivity, thermal conductivity, moisture state, pore structure, and mechanical properties [40]. At the element level, relevant descriptors include temperature difference, specimen geometry, electrode configuration, load condition, internal resistance, response time, and signal stability [67,148]. At the application level, the intended task should be specified, together with evidence of whether the element can provide a useable signal, store intermittent energy, activate a low-power component, or retain function after environmental exposure.

Several descriptors are especially important for comparison across studies, including accessible temperature gradient, heat-flow condition, load resistance, internal resistance, humidity condition, electrode material, contact method, testing duration, and retention after thermal or humidity cycling [149]. Without these descriptors, open-circuit voltage or short-term maximum power alone provides limited information about practical device performance. More consistent reporting would help move geopolymer thermoelectric binders from laboratory materials toward more stable, low-power, structure-integrated thermoelectric components.

6. Emerging opportunities and research roadmap

The preceding sections show that geopolymer thermoelectrics are moving from material-level response toward device-related functions, but the field has not yet formed a predictive design framework [20]. Future progress should focus less on repeating isolated performance demonstrations and more on building methods that make transport behavior interpretable, material design transferable, and device functions service-relevant [149]. In this context, several emerging directions deserve particular attention, including operation-coupled transport diagnostics, pore-interface programming, task-defined device architectures, and shared evidence for field validation.

6.1. Operation-coupled transport diagnostics for mixed ionic/electronic systems

A major opportunity lies in moving from post-test mechanism interpretation to operation-coupled transport diagnostics. Current studies often infer ionic thermodiffusion, interfacial polarization, or electronic leakage-related contributions from separate measurements. Future work could instead combine temperature-gradient output tests with time-resolved voltage/current recording and impedance spectroscopy under defined moisture and electrode conditions [57,81]. This would help examine voltage evolution, internal resistance, and interfacial response under the same thermal protocol, rather than interpreting them from independent tests alone [115].

Thermal and moisture states should also be recorded as part of the same testing framework. Infrared thermography or embedded thermocouples can help verify the actual thermal field across the specimen, while controlled-humidity testing and mass-change monitoring can provide practical information on bulk moisture evolution during heating, drying, or re-wetting [67,150]. Where leaching or environmental exposure is involved, post-exposure elemental mapping, leachate chemistry, or extractable alkali analysis may provide supporting evidence for changes in alkali distribution or alkali loss [151]. These methods are not a direct in situ visualization of mobile ions, but they can help reduce the ambiguity between transient polarization, quasi-stable thermovoltage, leakage-related contributions, and moisture-related changes during operation.

This direction is especially important for composites containing conductive fillers. In these systems, fillers may improve effective electrical conductivity, but they can also alter ion redistribution, moisture continuity, and interfacial stability [20]. Combining time-resolved output data with impedance response and moisture/thermal-field information would provide a more constrained basis for assessing whether a filler contributes to useful mixed transport or mainly introduces parallel electronic pathways. This could help move the field from qualitative mechanism assignment toward more quantitative interpretation of device-relevant response.

6.2. Pore-interface programming beyond empirical mix design

A second opportunity is to treat the pore network and electrode-adjacent region as programmable design spaces. Previous studies have adjusted precursor type, activator chemistry, filler content, and porosity, but these variables are often optimized empirically. Future materials design should focus on creating pore-interface environments that support ion-mediated thermovoltage generation while preserving moisture stability and mechanical integrity [152].

Possible strategies include mesopore-rich frameworks with controlled connectivity, internal water-retaining phases, ion-buffering additives, chemically stable electrode interlayers, and graded contact regions. These approaches should not aim for a single universal pore size or composition [107,152]. Their value lies in providing design principles that can be adapted to different geopolymer and alkali-activated systems. In this sense, pore-interface programming may become a bridge between binder chemistry and device stability.

6.3. Task-defined device architectures for infrastructure functions

Geopolymer thermoelectrics are unlikely to develop along the same path as conventional high-power thermoelectric modules. Their more realistic opportunity lies in low-power, structure-integrated functions. Future device architectures should therefore be designed from the intended task, such as thermal-gradient sensing, event-triggered warning, intermittent capacitor charging, or auxiliary power for low-duty-cycle sensor nodes [20].

This task-defined approach changes the role of material optimization. A large apparent Seebeck coefficient is useful only when it can be collected as a stable signal under practical boundary conditions [153]. For many infrastructure applications, a moderate but repeatable output may be more valuable than a larger response obtained under ideal laboratory gradients [154]. Future studies should connect material formulation, element geometry, interface design, and packaging strategy to a clearly defined device task.

6.4. Shared datasets and field-relevant validation

A further opportunity is to build cumulative evidence across laboratories and material systems. At this stage, a rigid standard may be premature, but shared minimum descriptors would make reported results more reusable. These descriptors should include material composition, moisture condition, element geometry, electrode configuration, temperature gradient, load condition, testing duration, and retention after environmental exposure [153].

Field-relevant validation is also needed to move beyond short-term laboratory demonstrations. Building envelopes, pavements, tunnels, and underground structures provide fluctuating heat input and changing moisture histories, which cannot be fully represented by constant laboratory gradients. Pilot-scale tests, even with low output, would be valuable if they report stable signals, environmental history, and device retention. As comparable datasets accumulate, data-assisted analysis may help identify relationships between binder design, device configuration, exposure history, and functional output [20,155,156].

Overall, future research on geopolymer thermoelectrics should move beyond incremental optimization of isolated parameters and focus on approaches that improve interpretability, transferability, and service relevance. Operation-coupled transport diagnostics can support more quantitative understanding of mixed ionic/electronic behavior, while pore-interface programming may help convert empirical formulation into more transferable design principles. Task-defined device architectures can align material response with realistic infrastructure functions, and shared datasets with field-relevant validation can make progress more reproducible and cumulative. These directions provide a practical route toward stable, low-power, structure-integrated thermoelectric components [157–159].

7. Conclusions

Geopolymer-based thermoelectric materials represent an emerging research direction linking construction materials, ion-mediated transport, and low-grade heat utilization. This review summarizes their binder-level mechanisms, performance-regulation strategies, device-integration challenges, and sustainability implications. Based on the literature reviewed in this work, several key conclusions can be drawn:

(1) Geopolymers exhibit intrinsic characteristics that support thermoelectric functionality. As ion-containing aluminosilicate binders, geopolymer systems generally show higher apparent Seebeck coefficients than conventional cementitious matrices, suggesting their potential as material platforms for structure-integrated thermoelectric applications in construction environments.

(2) The thermoelectric behavior of geopolymers is closely related to their binder structure and transport characteristics. The charged aluminosilicate framework, mobile alkali ions, connected pore solution, moisture state, and electrode boundary regions collectively give rise to an ion-dominated mixed transport regime. In hydrated or partially saturated geopolymer binders, ionic thermodiffusion, pore-solution redistribution, and ion–matrix interactions are expected to make the primary contribution to the apparent thermovoltage. Electronic pathways introduced by conductive fillers, redox-active phases, or severe drying can modify this ion-dominated response by adding parallel or filler-mediated transport contributions.

(3) Performance improvement in geopolymer thermoelectrics requires coupled optimization rather than single-parameter enhancement. Apparent Seebeck coefficient, effective electrical conductivity, thermal conductivity, moisture state, pore structure, filler connectivity, and interfacial processes are strongly interdependent. Conductive fillers can improve electrical conductivity, but may also alter apparent thermopower, thermal transport, moisture continuity, and mechanical performance. Similarly, pore engineering can reduce thermal conductivity but may disrupt ion-transport pathways or accelerate drying. Therefore, ZT and power factor should be interpreted together with device-relevant descriptors such as accessible temperature difference, internal resistance, response stability, humidity condition, and retention after environmental cycling.

(4) A clear gap remains between material-level characterization and device-level deployment. Existing studies have demonstrated thermovoltage generation, sensing response, series connection, and small module-like outputs, but most systems remain at the proof-of-concept stage. Interfaces, load matching, moisture-regulated packaging, long-term durability, scalable architectures, and operation under realistic fluctuating temperature and humidity conditions remain insufficiently validated. Device-level sustainability assessment is also needed because the carbon and energy burden depends on the binder, activators, conductive fillers, electrodes, auxiliary components, and device geometry.

(5) The most realistic near-term applications are low-power and structure-integrated functions. Given their current output levels and moisture-sensitive transport behavior, geopolymer thermoelectrics are unlikely to replace high-efficiency commercial thermoelectric modules for primary power generation. Their more plausible role lies in temperature-gradient sensing, distributed thermal monitoring, damage- or event-triggered signals, and intermittent auxiliary power for low-duty-cycle devices in construction environments. Progress toward these applications will require operation-coupled transport diagnostics, pore-interface design, durable packaging, shared reporting descriptors, and field-relevant validation.

CRediT authorship contribution statement

Zhiyang Pei: Writing – original draft. **Hanyun Hu:** Writing – original draft, Writing – review & editing. **Jiaming Gu:** Data curation, Visualization. **Jingming Cai:** Project administration, Supervision. **Y.X. Zhang:** Conceptualization, Supervision.

Declaration of competing interest

The authors declare that they have no known competing financial interests or personal relationships that could have appeared to influence the work reported in this paper.

Acknowledgments

This work was supported by the Smart Grid-National Science and Technology Major Project (2030) [grant number 2026ZD0809700] and Zhishan Young Scholars Program of Southeast University [grant number 2242025RCB0008].

Data availability

Data will be made available on request.

References

[1] Intergovernmental Panel on Climate Change (IPCC), Climate Change 2021 – The Physical Science Basis: Working Group I Contribution to the Sixth Assessment Report of the Intergovernmental Panel on Climate Change, Cambridge University Press, Cambridge (2023) 1–16, https://doi.org/10.1017/9781009157896.
[2] International Energy Agency (IEA), Global Energy Review 2025, IEA, Paris, 2025. https://www.iea.org/reports/global-energy-review-2025.
[3] A. Sohrabi, S. Liu, E. Cuce, Y. Shen, S.Y. Khan, M. Kumar, Utilization of low-grade thermal energy for residential applications: a review of the existing and potential technologies, Sustain. Energy Rev. 219 (2025) 115832, https://doi.org/10.1016/j.rser.2025.115832.
[4] K. Deilami, M. Kamruzzaman, Y. Liu, Urban heat island effect: a systematic review of spatio-temporal factors, data, methods, and mitigation measures, Int. J. Appl. Earth Obs. Geoinf. 67 (2018) 30–42, https://doi.org/10.1016/j.jag.2017.12.009.
[5] M. Roberts, C. Deuskar, N. Jones, J. Park, Unlivable: What the Urban Heat Island Effect Means for East Asia's Cities, World Bank, 2023, https://doi.org/10.1596/40771. Washington, DC.
[6] USGCRP, Climate Science Special Report: Fourth National Climate Assessment, U. S. Global Change Research Program, Washington, DC I (2017), https://doi.org/10.7930/J0J964J6.
[7] V.J. Reddy, N.P. Hariram, M.F. Ghazali, S. Kumarasamy, Pathway to sustainability: an overview of renewable energy integration in building systems, Sustainability 16 (2024) 638, https://doi.org/10.3390/su16020638.
[8] H. Jiang, L. Yao, J. Qin, Y. Bai, M. Brandt, X. Lian, S.J. Davis, N. Lu, W. Zhao, T. Liu, C. Zhou, Globally interconnected solar-wind system addresses future electricity demands, Nat. Commun. 16 (2025) 4523, https://doi.org/10.1038/s41467-025-59879-9.
[9] K. Kull, B. Asad, M.A. Khan, M.U. Naseer, A. Kallaste, T. Vaimann, Faults, failures, reliability, and predictive maintenance of grid-connected solar systems: a comprehensive review, Appl. Sci. 15 (2025) 11461, https://doi.org/10.3390/app152111461.
[10] S.B. Riffat, X. Ma, Thermoelectrics: a review of present and potential applications, Appl. Therm. Eng. 23 (2003) 913–935, https://doi.org/10.1016/s1359-4311(03)00012-7.
[11] Y. Jia, Q. Jiang, H. Sun, P. Liu, D. Hu, Y. Pei, W. Liu, X. Crispin, S. Fabiano, Y. Ma, Y. Cao, Wearable thermoelectric materials and devices for self-powered electronic systems, Adv. Mater. 33 (2021) e2102990, https://doi.org/10.1002/adma.202102990.
[12] M.A. Zoui, S. Bentouba, J.G. Stocholm, M. Bourouis, A review on thermoelectric generators: progress and applications, Energies 13 (2020) 3606, https://doi.org/10.3390/en13143606.
[13] A. Álvarez-Carulla, A. Saiz-Vela, M. Puig-Vidal, J. López-Sánchez, J. Colomer-Farrarons, P.L. Miribel-Català, High-efficient energy harvesting architecture for self-powered thermal-monitoring wireless sensor node based on a single thermoelectric generator, Sci. Rep. 13 (2023) 1637, https://doi.org/10.1038/s41598-023-28378-6.
[14] S.L.Y. Win, Y.-C. Chiang, T.-L. Huang, C.-M. Lai, Thermoelectric generator applications in buildings: a review, Sustainability 16 (2024) 7585, https://doi.org/10.3390/su16177585.
[15] I.T. Witting, T.C. Chasapis, F. Ricci, M. Peters, N.A. Heinz, G. Hautier, G. J. Snyder, The thermoelectric properties of bismuth telluride, Adv. Electron. Mater. 5 (2019) 1800904, https://doi.org/10.1002/aelm.201800904.
[16] T. Cao, X.-L. Shi, M. Li, B. Hu, W. Chen, W.-D. Liu, W. Lyu, J. MacLeod, Z.-G. Chen, Advances in bismuth-telluride-based thermoelectric devices: progress and challenges, eScience 3 (2023) 100122, https://doi.org/10.1016/j.esci.2023.100122.
[17] S. LeBlanc, S.K. Yee, M.L. Scullin, C. Dames, K.E. Goodson, Material and manufacturing cost considerations for thermoelectrics, Renew. Sustain. Energy Rev. 32 (2014) 313–327, https://doi.org/10.1016/j.rser.2013.12.030.
[18] H.J. Goldsmid, Bismuth telluride and its alloys as materials for thermoelectric generation, Materials 7 (2014) 2577–2592, https://doi.org/10.3390/ma7042577.
[19] Z. Bu, X. Zhang, Y. Hu, Z. Chen, S. Lin, W. Li, C. Xiao, Y. Pei, A record thermoelectric efficiency in tellurium-free modules for low-grade waste heat recovery, Nat. Commun. 13 (2022) 237, https://doi.org/10.1038/s41467-021-27916-y.
[20] W. Li, C. Du, L. Liang, G. Chen, Cement-based thermoelectric materials, devices and applications, Nano-Micro Lett. 18 (2026) 29, https://doi.org/10.1007/s40820-025-01866-2.
[21] X. Liu, R. Jani, E. Orisakwe, C. Johnston, P. Chudzinski, M. Qu, B. Norton, N. Holmes, J. Kohanoff, L. Stella, H. Yin, K. Yazawa, State of the art in composition, fabrication, characterization, and modeling methods of cement-based thermoelectric materials for low-temperature applications, Renew. Sustain. Energy Rev. 137 (2021) 110361, https://doi.org/10.1016/j.rser.2020.110361.
[22] V.P. Singh, M. Kumar, R.S. Srivastava, R. Vaish, Thermoelectric energy harvesting using cement-based composites: a review, mater, Today Energy 21 (2021) 100714, https://doi.org/10.1016/j.mtener.2021.100714.
[23] J. Wei, Y. Fan, L. Zhao, F. Xue, L. Hao, Q. Zhang, Thermoelectric properties of carbon nanotube reinforced cement-based composites fabricated by compression shear, Ceram. Int. 44 (2018) 5829–5833, https://doi.org/10.1016/j.ceramint.2018.01.074.
[24] J. Cai, J. Tan, X. Li, Thermoelectric behaviors of fly ash and metakaolin based geopolymer, Constr. Build. Mater. 237 (2020) 117757, https://doi.org/10.1016/j.conbuildmat.2019.117757.
[25] Y.-S. Wang, Y. Alrefaei, J.-G. Dai, Silico-aluminophosphate and alkali-aluminosilicate geopolymers: a comparative review, Front. Mater. 6 (2019) 106, https://doi.org/10.3389/fmats.2019.00106.
[26] B. Kim, S. Lee, Review on characteristics of metakaolin-based geopolymer and fast setting, J. Korean Ceram. Soc. 57 (2020) 368–377, https://doi.org/10.1007/s43207-020-00043-y.
[27] A.M. Elgarahy, A. Maged, M.G. Eloffy, M. Zahran, S. Kharbish, K.Z. Elwakeel, A. Bhatnagar, Geopolymers as sustainable eco-friendly materials: classification, synthesis routes, and applications in wastewater treatment, Sep. Purif. Technol. 324 (2023) 124631, https://doi.org/10.1016/j.seppur.2023.124631.
[28] J. Li, B.W.Y. Tay, J. Lei, E.-H. Yang, Experimental investigation of seebeck effect in metakaolin-based geopolymer, Constr. Build. Mater. 272 (2021) 121615, https://doi.org/10.1016/j.conbuildmat.2020.121615.
[29] P. Hotěk, L. Fiala, R. Černý, Thermoelectric properties of metashale geopolymer mortar doped with graphite powder, J. Phys., Conf. Ser. 2628 (2023) 012006, https://doi.org/10.1088/1742-6596/2628/1/012006.
[30] E.E. Sánchez Díaz, V.A. Escobar Barrios, Development and use of geopolymers for energy conversion: an overview, Constr. Build. Mater. 315 (2022) 125774, https://doi.org/10.1016/j.conbuildmat.2021.125774.
[31] S.I. Basha, S.S. Shah, D.-Y. Yoo, Advancements in thermoelectric properties of cement and geopolymer composites reinforced with carbon-based nanomaterials, J. Build. Eng. 104 (2025) 112312, https://doi.org/10.1016/j.jobe.2025.112312.
[32] J. Davidovits, Geopolymers: inorganic polymeric new materials, J. Therm. Anal. 37 (1991) 1633–1656, https://doi.org/10.1007/bf01912193.
[33] E. Ekinci, F. Kantarcı, M.M. Maraş, E. Ekinci, İ. Türkmen, R. Demirboğa, Historiography, current practice and future perspectives: a critical review of geopolymer binders, Sustainability 17 (2025) 9204, https://doi.org/10.3390/su17209204.
[34] Z. Jwaida, A. Dulaimi, N. Mashaan, M.A. Othuman Mydin, Geopolymers: the green alternative to traditional materials for engineering applications, Infrastructure 8 (2023) 98, https://doi.org/10.3390/infrastructures8060098.
[35] B. Kanagaraj, E. Lubloy, N. Anand, V. Hlavicka, T. Kiran, Investigation of physical, chemical, mechanical, and microstructural properties of cement-less concrete – state-of-the-art review, Constr. Build. Mater. 365 (2023) 130020, https://doi.org/10.1016/j.conbuildmat.2022.130020.
[36] R. Mohamed, M.M.A.B. Abdullah, R.A. Razak, T.L. Lee, T. Imjai, M.A.O. Mydin, Z. Yahya, P. Arokiasamy, D.L.C. Hao, Review: geopolymers for fire protection applications, J. Mater. Sci. 60 (2025) 18678–18709, https://doi.org/10.1007/s10853-025-11496-z.
[37] I. Lecomte, C. Henrist, M. Liégeois, F. Maseri, A. Rulmont, R. Cloots, (Micro)-structural comparison between geopolymers, alkali-activated slag cement and Portland cement, J. Eur. Ceram. Soc. 26 (2006) 3789–3797, https://doi.org/10.1016/j.jeurceramsoc.2005.12.021.
[38] P. Cong, R. Du, H. Gao, Z. Chen, Comparison and assessment of carbon dioxide emissions between alkali-activated materials and OPC cement concrete, J. Traffic Transport. Eng. 11 (2024) 918–938, https://doi.org/10.1016/j.jtte.2023.07.011.
[39] T. Luukkonen, Alkali-activated materials in environmental technology: introduction, in: T. Luukkonen (Ed.), Alkali-Activated Materials in Environmental Technology Applications, Woodhead Publishing, 2022, pp. 1–12, https://doi.org/10.1016/B978-0-323-88438-9.00011-9.
[40] Y. Yuan, J. Cai, X. Xi, N. Ukrainczyk, Y. Wang, Z. Pei, Y. Zhang, A. Weidenkaff, W. Xie, Advancing the mechanical and thermoelectric properties of geopolymers for sustainable architectureh, Small 21 (2025) 2408048, https://doi.org/10.1002/smll.202408048.

[41] J.G.S. Van Jaarsveld, J.S.J. Van Deventer, A. Schwartzman, The potential use of geopolymeric materials to immobilise toxic metals: part II. Material and leaching characteristics, Miner. Eng. 12 (1999) 75–91, https://doi.org/10.1016/S0892-6875(98)00121-6.
[42] P. Duxson, J.L. Provis, G.C. Lukey, S.W. Mallicoat, W.M. Kriven, J.S.J. van Deventer, Understanding the relationship between geopolymer composition, microstructure and mechanical properties, Colloids Surf., A 269 (2005) 47–58, https://doi.org/10.1016/j.colsurfa.2005.06.060.
[43] M. Ben Haha, G. Le Saout, F. Winnefeld, B. Lothenbach, Influence of activator type on hydration kinetics, hydrate assemblage and microstructural development of alkali activated blast-furnace slags, Cement Concr. Res. 41 (2011) 301–310, https://doi.org/10.1016/j.cemconres.2010.11.016.
[44] T. Jiang, Z. Liu, X. Tian, J. Wu, L. Wang, Review on the impact of metakaolin-based geopolymer's reaction chemistry, nanostructure and factors on its properties, Constr. Build. Mater. 412 (2024) 134760, https://doi.org/10.1016/j.conbuildmat.2023.134760.
[45] W.M. Kriven, C. Leonelli, J.L. Provis, A.R. Boccaccini, C. Attwell, V.S. Ducman, C. Ferone, S. Rossignol, T. Luukkonen, J.S.J. van Deventer, J.V. Emiliano, J. E. Lombardi, Why geopolymers and alkali-activated materials are key components of a sustainable world: a perspective contribution, J. Am. Ceram. Soc. 107 (2024) 5159–5177, https://doi.org/10.1111/jace.19828.
[46] J. Matsimbe, M. Dinka, D. Olukanni, I. Musonda, Geopolymer: a systematic review of methodologies, Materials 15 (2022) 6852, https://doi.org/10.3390/ma15196852.
[47] H.A. Hossein, A.A. El-Kheshen, M.F. Zawrah, Influence of silica-fume's addition technique and curing conditions on microstructure, physical and mechanical properties of geopolymer, Sci. Rep. 15 (2025) 38486, https://doi.org/10.1038/s41598-025-23157-x.
[48] Z. Xu, J. Yue, G. Pang, R. Li, P. Zhang, S. Xu, Influence of the activator concentration and solid/liquid ratio on the strength and shrinkage characteristics of alkali-activated slag geopolymer pastes, Adv. Civ. Eng. 2021 (2021) 6631316, https://doi.org/10.1155/2021/6631316.
[49] H. Ma, S. Li, M. Su, J. Feng, Research on thermoelectric seebeck effect and water-ion interaction mechanism of alkali-activated fly ash/slag materials, J. Build. Eng. 113 (2025) 114082, https://doi.org/10.1016/j.jobe.2025.114082.
[50] M. Sambucci, A. Sibai, M. Valente, Recent advances in geopolymer technology. A potential eco-friendly solution in the construction materials industry: a review, J. Compos. Sci. 5 (2021) 109, https://doi.org/10.3390/jcs5040109.
[51] L. Yao, D. Yang, Q. Tao, Z. Zhang, J. Luo, Y. Yan, X. Tang, Accelerated measurement of electrical resistivity and Seebeck coefficient for thin-layer thermoelectric materials, Meas. Sci. Technol. 34 (2023) 095908, https://doi.org/10.1088/1361-6501/acde00.
[52] J. Cai, X. Li, Thermoelectric properties of geopolymers with the addition of nano-silicon carbide (SiC) powder, Ceram. Int. 47 (2021) 19752–19759, https://doi.org/10.1016/j.ceramint.2021.03.313.
[53] P. Hotěk, L. Fiala, Thermoelectric properties of multifunctional metashale mortar with carbon fiber dust, J. Phys., Conf. Ser. 2911 (2024) 012009, https://doi.org/10.1088/1742-6596/2911/1/012009.
[54] L.-P. Guo, B.-C. Lyu, J.-O. He, J.-T. Lu, B. Chen, Mechanical and thermoelectric properties of high ductility geopolymer composites with nano zinc oxide and red mud, Constr. Build. Mater. 455 (2024) 139173, https://doi.org/10.1016/j.conbuildmat.2024.139173.
[55] R. Piao, D. Lee, S.Y. Woo, J.-W. Jeong, S.Y. Hiew, S.-J. Lee, D.-Y. Yoo, Carbon material-based thermoelectric ultra-high-performance alkali-activated concrete, Compos. Part B Eng. 297 (2025) 112279, https://doi.org/10.1016/j.compositesb.2025.112279.
[56] S. Jeon, N. Das, E.-H. Yang, Unveiling thermoelectricity of metakaolin-based geopolymer for sustainable energy harvesting, Constr. Build. Mater. 501 (2025) 144275, https://doi.org/10.1016/j.conbuildmat.2025.144275.
[57] G. Goracci, M.B. Ogundiran, M. Barzegar, A. Iturrospe, A. Arbe, J.S. Dolado, Kaolin clay-based geopolymer for ionic thermoelectric energy harvesting, ACS Omega 9 (2024) 13728–13737, https://doi.org/10.1021/acsomega.3c08257.
[58] J. Cai, Y. Yuan, X. Xi, N. Ukrainczyk, L. Pan, Y. Wang, J. Pan, Unveiling the remarkable potential of geopolymer-based materials by harnessing manganese dioxide incorporation, Small 20 (2024) 2305360, https://doi.org/10.1002/smll.202305360.
[59] T. Liang, S. Wang, D. Yan, Y. Liu, S. Chen, Enhancing thermoelectric performance of geopolymers via glass bead doping to regulate pore structure, Constr. Build. Mater. 496 (2025) 143740, https://doi.org/10.1016/j.conbuildmat.2025.143740.
[60] S. Wang, J. Mao, J. Lin, S. Chen, Y. Liu, D. Yan, Dissecting the role of geopolymer-electrode interfaces in ionic thermoelectrics: electrochemical activity and energy-level matching governing Seebeck behavior, Cem. Concr. Compos. 167 (2026) 106444, https://doi.org/10.1016/j.cemconcomp.2025.106444.
[61] G. Karalis, M. Liebscher, J. Mersch, J. Zhao, K.H. Ly, P. Machata, T. Köberle, M. Micusik, L. Tzounis, I. Weidinger, C. Cherif, V. Mechtcherine, Carbon nanotube fibers as efficient p- and n-type thermoelements within geopolymers: a route for large-scale thermal energy harvesting from building structures, Cem. Concr. Compos. 153 (2024) 105699, https://doi.org/10.1016/j.cemconcomp.2024.105699.
[62] G. Karalis, J. Zhao, T. Köberle, V. Mechtcherine, M. Liebscher, Temperature sensing performance of doped continuous carbon nanofiber filament-based thermocouples integrated in geopolymer-based mortar, Mater. Today Commun. 47 (2025) 113235, https://doi.org/10.1016/j.mtcomm.2025.113235.
[63] A. Santos, S. Andrejkovičová, F. Almeida, F. Rocha, Thermoelectric properties of geopolymers with iron ore mine waste: a case study for energy management, Ceram. Int. 50 (2024) 36112–36125, https://doi.org/10.1016/j.ceramint.2024.06.424.
[64] P. Hotěk, L. Fiala, Thermoelectric properties of metashale geopolymer with graphite powder in the dry and wet state, AIP Conf. Proc. 3315 (2025) 160003, https://doi.org/10.1063/5.0286174.
[65] P. Hotěk, L. Fiala, R. Černý, Design of thermoelectric geopolymer composite with carbonaceous admixture, AIP Conf. Proc. 3269 (2025) 030003, https://doi.org/10.1063/5.0247357.
[66] P. Hotěk, P. Konrád, L. Fiala, Thermoelectric properties of alkali-activated metashale composite with graphite powder, AIP Conf. Proc. 3094 (2024) 120003, https://doi.org/10.1063/5.0210476.
[67] M. Davoodabadi, I. Vareli, M. Liebscher, L. Tzounis, M. Sgarzi, A. Paipetis, J. Yang, G. Cuniberti, V. Mechtcherine, Thermoelectric energy harvesting from single-walled carbon nanotube alkali-activated nanocomposites produced from industrial waste materials, Nanomaterials 11 (2021) 1095, https://doi.org/10.3390/nano11051095.
[68] J. Cai, Y. Yuan, L. Pan, Z. Pei, Y. Zhang, X. Xi, N. Ukrainczyk, E.A.B. Koenders, L. Zhang, Y.X. Zhang, J. Pan, Y. Wang, W. Xie, Intelligent thermoelectric sensing with sustainable strain-hardening geopolymeric composites, Small Sci. 5 (2025) 2400520, https://doi.org/10.1002/smsc.202400520.
[69] M. Barzegar, G. Goracci, P. Martauz, J.S. Dolado, Sustainable geopolymer concrete for thermoelectric energy harvesting, Constr. Build. Mater. 411 (2024) 134398, https://doi.org/10.1016/j.conbuildmat.2023.134398.
[70] X. Qu, T. Guo, J. Cai, Y. Hu, B.-T. Huang, T. Xie, Characterization and analysis of electrothermal, thermoelectric, and current discharge properties of alkali-activated materials: implications for energy conversion, Cem. Concr. Compos. 159 (2025) 105987, https://doi.org/10.1016/j.cemconcomp.2025.105987.
[71] H.M. Park, S. Park, I.-J. Shon, G.M. Kim, S. Hwang, M.W. Lee, B. Yang, Influence of Portland cement and alkali-activated slag binder on the thermoelectric properties of the p-type composites with MWCNT, Constr. Build. Mater. 292 (2021) 123393, https://doi.org/10.1016/j.conbuildmat.2021.123393.
[72] P. Duxson, A. Fernández-Jiménez, J.L. Provis, G.C. Lukey, A. Palomo, J.S.J. van Deventer, Geopolymer technology: the current state of the art, J. Mater. Sci. 42 (2007) 2917–2933, https://doi.org/10.1007/s10853-006-0637-z.
[73] M.R. Sadat, S. Bringuier, K. Muralidharan, K. Runge, A. Asaduzzaman, L. Zhang, An atomistic characterization of the interplay between composition, structure and mechanical properties of amorphous geopolymer binders, J. Non-Cryst. Solids 434 (2016) 53–61, https://doi.org/10.1016/j.jnoncrysol.2015.11.022.
[74] O. Bortnovsky, J. Dědeček, Z. Tvarůžková, Z. Sobalík, J. Šubrt, Metal ions as probes for characterization of geopolymer materials, J. Am. Ceram. Soc. 91 (2008) 3052–3057, https://doi.org/10.1111/j.1551-2916.2008.02577.x.
[75] D. Hou, J. Zhang, W. Pan, Y. Zhang, Z. Zhang, Nanoscale mechanism of ions immobilized by the geopolymer: a molecular dynamics study, J. Nucl. Mater. 528 (2020) 151841, https://doi.org/10.1016/j.jnucmat.2019.151841.
[76] W. Zhang, J.-S. Li, X. Huang, Z. Chen, L. Lang, K. Huang, Unraveling the cation adsorption of geopolymer binder: a molecular dynamics study, Chemosphere 335 (2023) 139118, https://doi.org/10.1016/j.chemosphere.2023.139118.
[77] D. Zhao, S. Fabiano, M. Berggren, X. Crispin, Ionic thermoelectric gating organic transistors, Nat. Commun. 8 (2017) 14214, https://doi.org/10.1038/ncomms14214.
[78] J.L. Provis, A. Palomo, C. Shi, Advances in understanding alkali-activated materials, Cement Concr. Res. 78 (2015) 110–125, https://doi.org/10.1016/j.cemconres.2015.04.013.
[79] N. Jabeen, M. Muddasar, N. Menéndez, M.A. Nasiri, C.M. Gómez, M.N. Collins, R. Muñoz-Espí, A. Cantarero, M. Culebras, Recent advances in ionic thermoelectric systems and theoretical modelling, Chem. Sci. 15 (2024) 14122–14153, https://doi.org/10.1039/d4sc04158e.
[80] A. Hernández, J. Arcos, J. Martínez-Trinidad, O. Bautista, S. Sánchez, F. Méndez, Thermodiffusive effect on the local Debye-length in an electroosmotic flow of a viscoelastic fluid in a slit microchannel, Int. J. Heat Mass Tran. 187 (2022) 122522, https://doi.org/10.1016/j.ijheatmasstransfer.2022.122522.
[81] D. Zhao, A. Würger, X. Crispin, Ionic thermoelectric materials and devices, J. Energy Chem. 61 (2021) 88–103, https://doi.org/10.1016/j.jechem.2021.02.022.
[82] J. Liu, Y. Lu, X. Bai, P. Han, R. Xie, B. He, Strength characteristics and electrochemical impedance spectroscopy characterization of red mud-coal metakaolin geopolymers, Int. J. Electrochem. Sci. 15 (2020) 10694–10706, https://doi.org/10.20964/2020.11.03.
[83] D.B. Istuque, A.O. Sanches, M. Bortoletto, J.A. Malmonge, L. Soriano, M. V. Borrachero, J. Payá, M.M. Tashima, J.L. Akasaki, Impedance spectroscopy as a methodology to evaluate the reactivity of metakaolin based geopolymers, Materials 15 (2022) 8387, https://doi.org/10.3390/ma15238387.
[84] X. Zhang, L.-D. Zhao, Thermoelectric materials: energy conversion between heat and electricity, J. Materiomics 1 (2015) 92–105, https://doi.org/10.1016/j.jmat.2015.01.001.
[85] M. Saafi, K. Andrew, P.L. Tang, D. McGhon, S. Taylor, M. Rahman, S. Yang, X. Zhou, Multifunctional properties of carbon nanotube/fly ash geopolymeric nanocomposites, Constr. Build. Mater. 49 (2013) 46–55, https://doi.org/10.1016/j.conbuildmat.2013.08.007.
[86] S. Zhang, N. Ukrainczyk, A. Zaoui, E. Koenders, Electrical conductivity of geopolymer-graphite composites: percolation, mesostructure and analytical modeling, Constr. Build. Mater. 411 (2024) 134536, https://doi.org/10.1016/j.conbuildmat.2023.134536.
[87] W. Sekkal, A. Zaoui, Thermal and acoustic insulation properties in nanoporous geopolymer nanocomposite, Cem. Concr. Compos. 138 (2023) 104955, https://doi.org/10.1016/j.cemconcomp.2023.104955.

[88] J. Gao, Z. Yang, Z. Pi, Y. Wu, T. Bai, W. Jin, Preparation and performance study of a novel conductive geopolymer, Constr. Build. Mater. 411 (2024) 134388, https://doi.org/10.1016/j.conbuildmat.2023.134388.
[89] S. Jeon, N. Das, X.B. Tan, S. Lie, E. Julianto, L.H. Wong, E.-H. Yang, Investigation of the ion-electron hybrid thermoelectric properties of ultra-low carbon fiber-reinforced metakaolin-based geopolymer for sustainable energy harvesting building materials, J. Build. Eng. 124 (2026) 115982, https://doi.org/10.1016/j.jobe.2026.115982.
[90] P. Payakaniti, S. Pinitsoontorn, P. Thongbai, V. Amornkitbamrung, P. Chindaprasirt, Electrical conductivity and compressive strength of carbon fiber reinforced fly ash geopolymeric composites, Constr. Build. Mater. 135 (2017) 164–176, https://doi.org/10.1016/j.conbuildmat.2016.12.198.
[91] S. Zhang, J. Schuster, H. Frühauf-Wyllie, S. Arat, S. Yadav, J.J. Schneider, M. Stöckl, N. Ukrainczyk, E. Koenders, Conductive geopolymers as low-cost electrode materials for microbial fuel cells, ACS Omega 6 (2021) 28859–28870, https://doi.org/10.1021/acsomega.1c03805.
[92] T. Luo, H. Yuan, Q. Wang, Comparison the properties of carbon fiber-based Portland cement and alkali-activated fly ash/slag conductive cementitious composites, J. Build. Eng. 76 (2023) 107134, https://doi.org/10.1016/j.jobe.2023.107134.
[93] J. Han, J. Pan, X. Wang, J. Cai, L. Gu, J. Yang, Conductive behavior of engineered geopolymer composite with addition of carbon fiber and nano-carbon black, Ceram. Int. 49 (2023) 32035–32048, https://doi.org/10.1016/j.ceramint.2023.07.170.
[94] L. Wu, X. Li, S. Wang, T. Zhang, J. Yang, W. Zhang, L. Chen, J. Yang, Resonant level-induced high thermoelectric response in indium-doped GeTe, NPG Asia Mater. 9 (2017) e343, https://doi.org/10.1038/am.2016.203.
[95] N.A. Mohd Radzuan, A.B. Sulong, J. Sahari, A review of electrical conductivity models for conductive polymer composite, Int. J. Hydrogen Energy 42 (2017) 9262–9273, https://doi.org/10.1016/j.ijhydene.2016.03.045.
[96] S. Hanjitsuwan, S. Hunpratub, P. Thongbai, S. Maensiri, V. Sata, P. Chindaprasirt, Effects of NaOH concentrations on physical and electrical properties of high calcium fly ash geopolymer paste, Cem. Concr. Compos. 45 (2014) 9–14, https://doi.org/10.1016/j.cemconcomp.2013.09.012.
[97] X. Hu, C. Shi, X. Liu, Z. Zhang, Studying the effect of alkali dosage on microstructure development of alkali-activated slag pastes by electrical impedance spectroscopy (EIS), Constr. Build. Mater. 261 (2020) 119982, https://doi.org/10.1016/j.conbuildmat.2020.119982.
[98] R. Navarro, E. Zornoza, E.G. Alcocel, I. Sánchez, Use of impedance spectroscopy for the characterization of the microstructure of alkali activated SiMn slag: influence of activator and time evolution, J. Nondestruct. Eval. 42 (2023) 8, https://doi.org/10.1007/s10921-022-00918-6.
[99] E. Duque-Redondo, K. Yamada, E. Masoero, J. Bañuelos Prieto, H. Manzano, Adsorption and migration of Cs and Na ions in geopolymers and zeolites, Mater. Today Commun. 36 (2023) 106496, https://doi.org/10.1016/j.mtcomm.2023.106496.
[100] X. Ke, S.A. Bernal, T. Sato, J.L. Provis, Alkali aluminosilicate geopolymers as binders to encapsulate strontium-selective titanate ion-exchangers, Dalton Trans. 48 (2019) 12116–12126, https://doi.org/10.1039/c9dt02108f.
[101] W. Sheng, L. Chen, F. Zhang, H. Hu, Synergistic thermal conductivity enhancement in geopolymer–graphene aerogel composites through 3D structuring and gelation kinetics, Carbon Neutralization 4 (2025) e70067, https://doi.org/10.1002/cnl2.70067.
[102] M.F. Ali, M.M. Vijayalakshmi Natrajan, A review of geopolymer composite thermal properties, IOP Conf. Ser. Earth Environ. Sci. 822 (2021) 012051, https://doi.org/10.1088/1755-1315/822/1/012051.
[103] M.Y.J. Liu, U.J. Alengaram, M.Z. Jumaat, K.H. Mo, Evaluation of thermal conductivity, mechanical and transport properties of lightweight aggregate foamed geopolymer concrete, Energy Build. 72 (2014) 238–245, https://doi.org/10.1016/j.enbuild.2013.12.029.
[104] N.A. Jaya, L. Yun-Ming, H. Cheng-Yong, M.M.A.B. Abdullah, K. Hussin, Correlation between pore structure, compressive strength and thermal conductivity of porous metakaolin geopolymer, Constr. Build. Mater. 247 (2020) 118641, https://doi.org/10.1016/j.conbuildmat.2020.118641.
[105] P. Bazan, B. Figiela, B. Kozub, M. Łach, K. Mróz, M. Melnychuk, K. Korniejenko, Geopolymer foam with low thermal conductivity based on industrial waste, Materials 17 (2024) 6143, https://doi.org/10.3390/ma17246143.
[106] H. Karakaş, S. İlkentapar, U. Durak, E. Örklemez, S. Özuzun, O. Karahan, C. D. Atiş, Properties of fly ash-based lightweight-geopolymer mortars containing perlite aggregates: mechanical, microstructure, and thermal conductivity coefficient, Constr. Build. Mater. 362 (2023) 129717, https://doi.org/10.1016/j.conbuildmat.2022.129717.
[107] S. Chen, S. Ruan, Q. Zeng, Y. Liu, M. Zhang, Y. Tian, D. Yan, Pore structure of geopolymer materials and its correlations to engineering properties: a review, Constr. Build. Mater. 328 (2022) 127064, https://doi.org/10.1016/j.conbuildmat.2022.127064.
[108] P. Zhong, Z. Hu, M. Griffa, M. Wyrzykowski, J. Liu, P. Lura, Mechanisms of internal curing water release from retentive and non-retentive superabsorbent polymers in cement paste, Cement Concr. Res. 147 (2021) 106494, https://doi.org/10.1016/j.cemconres.2021.106494.
[109] D.M. Samuel, N. Inumerable, A. Stumpf, W.M. Kriven, Thermal conductivity of several geopolymer composites and discussion of their formulation, Int. J. Appl. Ceram. Technol. 20 (2023) 475–486, https://doi.org/10.1111/ijac.14200.
[110] T.A. Yemata, A.K.K. Kyaw, Y. Zheng, J. Xu, W.S. Chin, Q. Zhu, Y. Hayashi, Interface engineering in polymer thermoelectric composites: harnessing energy-filtering effects to overcome the Seebeck-conductivity trade-off, J. Mater. Chem. A 13 (2025) 35976–35998, https://doi.org/10.1039/D5TA05957G.
[111] O. Zmeškal, T. Lapčíková, K. Filipská, L. Fiala, Z. Pavlík, Thermoelectric properties of alkali-activated composites based on different precursors and carbonaceous admixtures, AIP Conf. Proc. 3315 (2025) 060004, https://doi.org/10.1063/5.0286294.
[112] T. Takabatake, K. Suekuni, T. Nakayama, E. Kaneshita, Phonon-glass electron-crystal thermoelectric clathrates: experiments and theory, Rev. Mod. Phys. 86 (2014) 669–716, https://doi.org/10.1103/RevModPhys.86.669.
[113] C. Zhao, Y. Wu, D. Song, X. Zhang, W. Ma, Moisture-gradient-enhanced ionic thermoelectrics, Nat. Commun. 16 (2025) 11099, https://doi.org/10.1038/s41467-025-66027-w.
[114] M. Fu, Z. Sun, Y. Yuan, K. Yue, Ionic thermoelectric materials based on the thermodiffusion effect: mechanism, advancements, and applications, Macromol. Chem. Phys. 226 (2025) 2400358, https://doi.org/10.1002/macp.202400358.
[115] S. Mardi, D. Zhao, N. Kim, I. Petsagkourakis, K. Tybrandt, A. Reale, X. Crispin, The interfacial effect on the open circuit voltage of ionic thermoelectric devices with conducting polymer electrodes, Adv. Electron. Mater. 7 (2021) 2100506, https://doi.org/10.1002/aelm.202100506.
[116] A.L. Sehnem, M. Janssen, On the time-dependent electrolyte Seebeck effect, J. Chem. Phys. 154 (2021) 164511, https://doi.org/10.1063/5.0045137.
[117] W. Le, W. Yang, W. Sheng, J. Shuai, Research progress of interfacial design between thermoelectric materials and electrode materials, ACS Appl. Mater. Interfaces 15 (2023) 12611–12621, https://doi.org/10.1021/acsami.2c21035.
[118] M. Liu, W. Li, Y. Pei, Screening metal diffusion barriers for thermoelectric Bi0.5Sb1.5Te3, Sci. China Mater. 67 (2024) 289–294, https://doi.org/10.1007/s40843-023-2696-1.
[119] M. Fu, Z. Sun, X. Liu, Z. Huang, G. Luan, Y. Chen, J. Peng, K. Yue, Highly stretchable, resilient, adhesive, and self-healing ionic hydrogels for thermoelectric application, Adv. Funct. Mater. 33 (2023) 2306086, https://doi.org/10.1002/adfm.202306086.
[120] R. Duan, X. Chai, Z. Zhang, Y. Zhao, Y. Li, Ionic hydrogels synthesized from ionic liquid/water binary solvent systems: demonstrating superior antifreeze and moisture retention capabilities for self-powered wearable strain-sensing applications, Chem. Eng. J. 527 (2026) 171610, https://doi.org/10.1016/j.cej.2025.171610.
[121] W. Zhao, T. Sun, Y. Zheng, Q. Zhang, A. Huang, L. Wang, W. Jiang, Tailoring intermolecular interactions towards high-performance thermoelectric ionogels at low humidity, Adv. Sci. 9 (2022) 2201075, https://doi.org/10.1002/advs.202201075.
[122] C. Liu, Z. Li, G. Ye, Mitigating the efflorescence of alkali-activated slag mortars by aluminosilicate-based lightweight fine aggregate, Cement Concr. Res. 195 (2025) 107917, https://doi.org/10.1016/j.cemconres.2025.107917.
[123] C. Liu, Z. Li, G. Ye, Mechanisms of efflorescence of alkali-activated slag, Cem. Concr. Compos. 155 (2025) 105811, https://doi.org/10.1016/j.cemconcomp.2024.105811.
[124] J. Wang, Y. Deng, C. Mou, J. Ding, J. Ni, X. Wan, Durability and degradation mechanisms of dredged clays stabilized with ternary geopolymer under cyclic drying-wetting environments, Bull. Eng. Geol. Environ. 84 (2025) 250, https://doi.org/10.1007/s10064-025-04298-9.
[125] H.S. Gökçe, Durability of slag-based alkali-activated materials: a critical review, J. Aust. Ceram. Soc. 60 (2024) 885–903, https://doi.org/10.1007/s41779-024-01011-z.
[126] M. Zhang, J. Chen, M. Cheng, L. Zhang, Q. Wen, Y. Wen, H. Zhou, Q. Fu, H. Deng, Long-term serviceable ionic thermoelectric hydrogel with temperature and moisture dual-driven waste energy harvesting capability, Small 21 (2025) 2501960, https://doi.org/10.1002/smll.202501960.
[127] Q. Lin, Y.-C. Chen, F. Chen, T. DeGanyar, H. Yin, Design and experiments of a thermoelectric-powered wireless sensor network platform for smart building envelope, Appl. Energy 305 (2022) 117791, https://doi.org/10.1016/j.apenergy.2021.117791.
[128] M. Guan, K. Wang, D. Xu, W.-H. Liao, Design and experimental investigation of a low-voltage thermoelectric energy harvesting system for wireless sensor nodes, Energy Convers. Manag. 138 (2017) 30–37, https://doi.org/10.1016/j.enconman.2017.01.049.
[129] B. Ding, Z. Pei, Z. Hu, J. Pan, J. Han, J. Cai, Thermoelectric properties of engineered geopolymer composites (EGC) with multiscale conductive filler design, J. Build. Eng. 123 (2026) 115903, https://doi.org/10.1016/j.jobe.2026.115903.
[130] E. Janowska-Renkas, M. Zdrojek, M. Kozioł, A. Kaliciak-Kownacka, Effect of composition of geopolymer composites containing fly ash and waste glass powder on their durability and resistivity demonstrated in presence of a nanocarbon additive in a form of graphene, Measurement 211 (2023) 112616, https://doi.org/10.1016/j.measurement.2023.112616.
[131] J.A. De Sousa, E. Sánchez-Villegas, C.O. Avci, A miniaturized transverse thermoelectric device for efficient energy harvesting and its capacitive storage, Adv. Mater. Technol. 10 (2025) e00770, https://doi.org/10.1002/admt.202500770.
[132] J. Zhao, L. Tong, B. Li, T. Chen, C. Wang, G. Yang, Y. Zheng, Eco-friendly geopolymer materials: a review of performance improvement, potential application and sustainability assessment, J. Clean. Prod. 307 (2021) 127085, https://doi.org/10.1016/j.jclepro.2021.127085.
[133] P. Baskaran, M. Rajasekar, Recent progress in thermoelectric devices and applications, Chem. Eng. J. 506 (2025) 159929, https://doi.org/10.1016/j.cej.2025.159929.

[134] K. Kannan, A. Abdul Rahim, Optimization of sustainable ternary low-carbon geopolymer binders using the best–worst multi-criteria decision-making method, Front. Built Environ. 12 (2026) 1748711, https://doi.org/10.3389/fbuil.2026.1748711.
[135] H. Ye, B. Zhu, P. Ping, Y. Lin, J. Cai, J. Pan, Mechanical performance, impact behavior and environmental assessment of coal furnace slag based low-carbon ultra-high performance engineered cementitious composites (UHP-ECC), J. Clean. Prod. 450 (2024) 141921, https://doi.org/10.1016/j.jclepro.2024.141921.
[136] B.C. Mendes, L.G. Pedroti, C.M.F. Vieira, J.M.F. Carvalho, J.C.L. Ribeiro, N. M. Albuini-Oliveira, I.K.R. Andrade, Evaluation of eco-efficient geopolymer using chamotte and waste glass-based alkaline solutions, Case Stud. Constr. Mater. 16 (2022) e00847, https://doi.org/10.1016/j.cscm.2021.e00847.
[137] Q. Li, M.R. Vogt, H. Wang, C. Monticelli, A. Zanelli, Life cycle assessment of roll-to-roll produced chemical vapor deposition graphene transparent electrodes towards copper foil recycling, J. Clean. Prod. 468 (2024) 143068, https://doi.org/10.1016/j.jclepro.2024.143068.
[138] D. Surovtseva, E. Crossin, R. Pell, L. Stamford, Toward a life cycle inventory for graphite production, J. Ind. Ecol. 26 (2022) 964–979, https://doi.org/10.1111/jiec.13234.
[139] V.K.K. Upadhyayula, D.E. Meyer, M.A. Curran, M.A. Gonzalez, Life cycle assessment as a tool to enhance the environmental performance of carbon nanotube products: a review, J. Clean. Prod. 26 (2012) 37–47, https://doi.org/10.1016/j.jclepro.2011.12.018.
[140] C. Qi, L. Ye, X. Ma, D. Yang, J. Hong, Life cycle assessment of the hydrometallurgical zinc production chain in China, J. Clean. Prod. 156 (2017) 451–458, https://doi.org/10.1016/j.jclepro.2017.04.084.
[141] A. Pakdel, A. Reilly, Life-cycle assessment of carbon footprint and energy intensity of thermoelectric generator production for near-room-temperature applications, Device 4 (2026) 101085, https://doi.org/10.1016/j.device.2026.101085.
[142] J. Wei, Y. Zhou, Y. Wang, Z. Miao, Y. Guo, H. Zhang, X. Li, Z. Wang, Z. Shi, A large-sized thermoelectric module composed of cement-based composite blocks for pavement energy harvesting and surface temperature reducing, Energy 265 (2023) 126398, https://doi.org/10.1016/j.energy.2022.126398.
[143] H.Y. Teah, T. Sato, K. Namiki, M. Asaka, K. Feng, S. Noda, Life cycle greenhouse gas emissions of long and pure carbon nanotubes synthesized via On-Substrate and fluidized-bed chemical vapor deposition, ACS Sustainable Chem. Eng. 8 (2020) 1730–1740, https://doi.org/10.1021/acssuschemeng.9b04542.
[144] X. Tang, Z. Li, W. Liu, Q. Zhang, C. Uher, A comprehensive review on Bi2Te3-based thin films: thermoelectrics and beyond, Interdiscip. Mater. 1 (2022) 88–115, https://doi.org/10.1002/idm2.12009.
[145] J. Dong, M. Chen, J. Wang, Recycling and optimum utilization of GFRP waste into low-carbon geopolymer paste for sustainable development, J. Build. Eng. 97 (2024) 110867, https://doi.org/10.1016/j.jobe.2024.110867.
[146] M. Nikravan, R. Firdous, D. Stephan, Life cycle assessment of alkali-activated materials: a systematic literature review, Low-carbon Mater. Green Construction 1 (2023) 13, https://doi.org/10.1007/s44242-023-00014-6.
[147] S. Sun, M. Li, X.-L. Shi, Z.-G. Chen, Advances in ionic thermoelectrics: from materials to devices, Adv. Energy Mater. 13 (2023) 2203692, https://doi.org/10.1002/aenm.202203692.
[148] N.P. Williams, J. Power, D. Trimble, S.M. O'Shaughnessy, An experimental evaluation of thermoelectric generator performance under cyclic heating regimes, Heat Mass Tran. 60 (2024) 1991–2003, https://doi.org/10.1007/s00231-022-03280-5.
[149] K.A. Borup, J. de Boor, H. Wang, F. Drymiotis, F. Gascoin, X. Shi, L. Chen, M. I. Fedorov, E. Müller, B.B. Iversen, G.J. Snyder, Measuring thermoelectric transport properties of materials, Energy Environ. Sci. 8 (2015) 423–435, https://doi.org/10.1039/c4ee01320d.
[150] T.J. Chidiac, N. Ukrainczyk, Z. Zhang, J.L. Provis, E. Koenders, Moisture transport properties of alkali-activated binders, Mater. Struct. 59 (2026) 116, https://doi.org/10.1617/s11527-026-03003-w.
[151] I. Bentegri, M. De Campos, A. Hasnaoui, C. Reeb, C. Albert-Mercier, C. Davy, D. Lambertin, Durability of alkali-activated materials in cementitious leaching environments, Results Eng. 29 (2026) 108698, https://doi.org/10.1016/j.rineng.2025.108698.
[152] Y. Choi, J.Y. Kim, B.-C. Kang, H. Kim, Perspectives on hydrogel-based ionic thermoelectrics: from mechanistic insights to wearable applications of thermo-diffusive ionic materials, Energy Mater 5 (2025) 500106, https://doi.org/10.20517/energymater.2025.50.
[153] E. Koo, H. Jang, Y.S. Jung, S. Park, S.-B. Kang, M.-W. Oh, S.H. Park, Development of a standard reference thermoelectric module: enhancing durability and reproducibility through metallic materials and geometric thermoelectric leg shapes, ACS Appl. Mater. Interfaces 17 (2025) 59571–59582, https://doi.org/10.1021/acsami.5c14320.
[154] D.D. Sarma, Essential considerations for reporting thermoelectric properties, ACS Energy Lett. 6 (2021) 3715–3718, https://doi.org/10.1021/acsenergylett.1c02043.
[155] L. Deng, X. Sui, Z. Hu, Y. Yuan, Z. Pei, Y.X. Zhang, W. Xie, L.L. Wang, J. Pan, J. Cai, Thermoelectric energy-harvesting concrete modules for multifunctional building elements, Cem. Concr. Compos. 171 (2026) 106648, https://doi.org/10.1016/j.cemconcomp.2026.106648.
[156] C. Li, Z. Pei, Y. Lin, W. Xie, N. Ukrainczyk, E.A.B. Koenders, J. Cai, Thermoelectric brick with solid–solid phase change materials for building-integrated energy harvesting: design, simulation, and global evaluation, Appl. Therm. Eng. 282 (2026) 128844, https://doi.org/10.1016/j.applthermaleng.2025.128844.
[157] H. Ran, M. Elchalakani, M.A. Sadakkathulla, J. Cai, T. Xie, Thermoelectric ultra-lightweight high-performance ECC using cenospheres and calcined petroleum coke, Constr. Build. Mater. 407 (2023) 133513, https://doi.org/10.1016/j.conbuildmat.2023.133513.
[158] H. Ran, M. Elchalakani, M.A. Sadakkathulla, S. Yehia, J. Cai, T. Xie, Thermoelectric engineered cementitious composites with low thermal conductivity for efficiency improvement of buildings, Energy Build. 317 (2024) 114390, https://doi.org/10.1016/j.enbuild.2024.114390.
[159] H. Ran, M. Elchalakani, Z. Hu, P. Ayough, M.A. Sadakkathulla, J. Cai, Self-sensing function and thermoelectric effect of engineered cementitious composites (ECC) with porous structures, Energy Build. 324 (2024) 114846, https://doi.org/10.1016/j.enbuild.2024.114846.